Presynaptic developmental plasticity allows robust sparse wiring of the *Drosophila* mushroom body

Najia A. Elkahlah[1, *], Jackson A. Rogow[2, *], and E. Josephine Clowney[1, $]

1. Department of Molecular, Cellular, and Developmental Biology, The University of Michigan, Ann Arbor, MI 48109, USA

2. Laboratory of Neurophysiology and Behavior, The Rockefeller University, New York, NY 10065, USA.

* These authors contributed equally to this work.

$ To whom correspondence should be addressed: jclowney@umich.edu

Abstract: In order to represent complex stimuli, principle neurons of associative learning regions receive combinatorial sensory inputs. Developmental wiring programs can produce innervation densities that vary by several orders of magnitude, such that cortical pyramidal cells receive on the order of 1000 inputs, while principle neurons of cerebellum-like structures receive <10 inputs. These innervation patterns are theorized to determine the number of distinct stimuli that can be represented and distinguished from one another in sensory processing regions, with sparse, combinatorial (or "distributed") innervation thought to optimize the complexity of representations in networks of limited size. How the convergence of combinatorial inputs to principle neurons of associative brain regions is established during development is unknown. Here, we explore the developmental patterning of sensory inputs to principle neurons of the *Drosophila melanogaster* mushroom body, a cerebellum-like structure required for olfactory learning. Individual mushroom body Kenyon cells receive only 3-10 of the 50 available olfactory projection neuron inputs through large, claw-like dendritic structures. By manipulating the ratio between pre- and post-synaptic cells, we find that convergence ratio is set by postsynaptic Kenyon cells: Kenyon cells produce largely fixed distributions of dendritic claws while presynaptic projection neurons exhibit extensive plasticity in their repertoire of presynaptic processes. Moreover, we show that sparse odor responses are preserved in mushroom bodies with severe reductions in cellular repertoires, suggesting that developmental specification of convergence ratio allows functional robustness.

Introduction: The environmental stimuli animals encounter on a day-to-day basis are extraordinarily numerous. Olfactory systems have evolved to cope with this diversity by maximizing the chemicals that can be detected, through the amplification of chemosensory receptor gene families, and through combinatorial coding, which expands representation capacity from the number of receptors in the genome to the number of combinations among them. The arthropod mushroom body is a cerebellum-like associative learning structure with a well-understood role in

42 representing sensory stimuli and associating sensory and contextual cues (Farris, 2011; Hige,
43 2018; Kennedy, 2015). While mushroom bodies of different insect species process information
44 from a variety of sensory modalities, 90% of Kenyon cell inputs in *Drosophila melanogaster* are
45 olfactory (Zheng et al., 2018). The mushroom body of each hemisphere has ~2000 Kenyon cells
46 (KCs), which are two synapses from the sensory periphery. Each olfactory receptor neuron in
47 the antennae of adult flies expresses one or two of 75 olfactory receptor genes encoded in the
48 genome. The axons of neurons expressing the same receptor converge on one of 50 glomeruli
49 in the antennal lobe. ~150 uniglomerular projection neurons (PNs) have dendrites in one of the
50 50 glomeruli and carry signals about distinct receptor channels to two regions of the proto-
51 cerebrum, the lateral horn and the mushroom body calyx (Figure 1A). PN inputs to the lateral
52 horn are thought to underlie innate behaviors, while inputs to the mushroom body allow flexible
53 learned association of odor stimuli with behavioral context (Chin et al., 2018; de Belle and Hei-
54 senberg, 1994; Fişek and Wilson, 2014; Jefferis et al., 2007; Ruta et al., 2010).
55
56 In the mushroom body calyx, the presynaptic sites of individual olfactory PNs cluster into multi-
57 synaptic boutons, with PNs of different types (innervating different glomeruli) producing con-
58 sistent, characteristic bouton numbers (Caron et al., 2013; Zheng et al., 2018). Each PN makes
59 1-20 boutons, and each bouton is wrapped by claws of ~10 KCs, such that each PN sends out-
60 put to between 10 and 200 of the 2000 KCs (Leiss et al., 2009). KCs in turn have 3-10 (average
61 of five) claws, which innervate boutons of various PNs (Caron et al., 2013; Gruntman and
62 Turner, 2013; Zheng et al., 2018). Each KC therefore receives innervation from only a minority
63 of the 50 incoming sensory channels, and different individual KCs receive different and relatively
64 unstructured combinations of inputs (Caron et al., 2013; Chabrol et al., 2015; Eichler et al.,
65 2017; Honegger et al., 2011; Huang et al., 2013; Ishikawa et al., 2015; Murthy et al., 2008;
66 Zheng et al., 2018). The sets of inputs to individual cells vary across hemispheres and likely
67 across individuals (Caron et al., 2013; Eichler et al., 2017; Honegger et al., 2011; Murthy et al.,

2008). Associative learning mechanisms operate at KC output synapses, in the mushroom body axonal lobes, to re-weight KC outputs depending on experience and shift animal behavior (Cohn et al., 2015; Handler et al., 2019; Hige et al., 2015; Owald and Waddell, 2015).

The mushroom body is a simplified and experimentally tractable example of an expansion layer, in which a set of sensory inputs is mapped combinatorially onto a much larger set of postsynaptic cells, increasing the dimensionality of sensory representations. Like the diversification of antibodies by V(D)J recombination, the diversification of sensory input combinations across KCs is thought to allow them to represent arbitrary odors, regardless of evolutionary experience. Neurons of many other expansion layers receive similarly few, or sparse, sensory inputs. These include the cerebellum proper, the electric organ of mormyrid fish, the dorsal cochlear nucleus, and the hippocampus (Bell et al., 2008; Keene and Waddell, 2007; Mugnaini et al., 1980). Cerebellar granule cells have an average of four large, claw-shaped dendrites that are innervated by clustered mossy fiber presynaptic sites in mossy fiber rosettes. The similar convergence ratios in the cerebellum and mushroom body (4 or 5 sensory inputs, respectively, per expansion layer cell) are thought to maximize dimensionality of sensory representations by optimizing the tradeoff between stimulus representation, which is maximized when expansion layer neurons receive large combinations of inputs, and stimulus separation, which is maximized when expansion layer neurons receive few inputs (Albus, 1971; Cayco-Gajic et al., 2017; Litwin-Kumar et al., 2017; Marr, 1969). The number of sensory inputs received by expansion layer neurons is thus a crucial parameter in sensory coding. How the density of inputs to expansion layer neurons is developmentally programmed is not understood in any system.

Innervation complexity more generally has been studied in the peripheral nervous system and in the developing mammalian cortex. In the peripheral nervous system, including the rabbit ciliary ganglion, vertebrate neuromuscular junction, and *Drosophila* larval body wall, postsynaptic cells

are thought to set wiring complexity cell-autonomously (Corty et al., 2016; Gibbins et al., 2003; Hume and Purves, 1983, 1981; Jan and Jan, 2010; Purves and Hume, 1981; Turney and Lichtman, 2012). In contrast, in the developing cortex, extracellular signals including BDNF play a strong role in influencing dendritic complexity, suggesting that presynaptic cells and glial also influence connectivity density (Kohara et al., 2003; McAllister et al., 1997, 1995; Purves, 1986). Therefore, while mechanisms acting in both pre- and post-synaptic cells *can* influence innervation complexity, there is a need to directly compare how pre- and post-synaptic cells influence one another.

We sought to ask how convergence ratio is set in the mushroom body calyx. By bidirectionally varying the populations of pre- and post-synaptic cells, we were able to make many different mushroom body aberrations. Across these conditions, we found a consistent pattern of compensations: the number of claws per KC remained largely constant, while the number of presynaptic boutons per olfactory PN varied bidirectionally and in response to changes of both the PN and KC populations. We therefore conclude that in this circuit, connectivity density is set by aspects of KC specification and is accomplished by flexible innervation of the calyx by PNs.

Results: In order to ask whether presynaptic olfactory PNs or postsynaptic KCs (or both) dictate sparse wiring density in the mushroom body calyx, we used a variety of methods to manipulate the ratio between pre- and post-synaptic cells during embryonic or larval stages, well before adult connections form in the pupa. Through a combination of genetic and pharmacological interventions, we were able to vary both cell populations up and down. In these four conditions, we then examined gross calyx anatomy in adult animals and, when possible, the processes of individual PNs and KCs. These experiments allowed us to ask which population of neurons would adjust its production of processes in response to the perturbation. As we will describe, in

119 all four cases, PNs adjusted their repertoire of presynaptic sites while KC claw number re-
120 mained similar to that of unmanipulated animals.
121
122 **Projection neurons reduce bouton number when Kenyon cell number is reduced**
123 First, we sought to reduce the KC population, to ask whether remaining cells would increase
124 their claw number to fully innervate incoming PN boutons, or whether PNs would scale down
125 their boutons to the KC repertoire. To do this, we took advantage of existing pharmacological
126 techniques for KC neuroblast ablation (de Belle and Heisenberg, 1994; Sweeney et al., 2012).
127 In the fly, four KC neuroblasts in each hemisphere produce ~500 KCs each (Ito et al., 1997). In
128 the early '90s, researchers found that while most neuroblasts pause their divisions for the first 8
129 hours after hatching, the KC neuroblasts continue to divide; if larvae are fed the mitotic poison
130 hydroxyurea during this time, KC neuroblasts can be specifically ablated (de Belle and Heisen-
131 berg, 1994). In these animals, lacking all KCs that receive olfactory inputs, olfactory learning is
132 abrogated while innate olfactory behaviors are spared (de Belle and Heisenberg, 1994). The
133 uniglomerular, excitatory olfactory PNs that innervate the MB calyx are produced by two neuro-
134 blasts, called lNB/BAlc and adNB/BAmv3 . Besides the KC neuroblasts, lNB/BAlc is the only
135 other neuroblast in the fly central nervous system dividing from 0-8h ALH and is thus also sus-
136 ceptible to HU ablation (Das et al., 2013; Ito and Hotta, 1992; Lovick et al., 2016; Lovick and
137 Hartenstein, 2015; Stocker et al., 1997; Sweeney et al., 2012).
138
139 While ablation of all eight KC neuroblasts (4/hemisphere) was used to demonstrate the role of
140 KCs in olfactory learning (de Belle and Heisenberg, 1994), we sought to perform more subtle
141 manipulations of the mushroom body cell populations. We generated animals in which PNs and
142 KCs were fluorescently labeled to facilitate scoring, and reduced the concentration and duration
143 of HU application, producing mushroom bodies with a variety of Kenyon cell complements, likely
144 due to sporadic loss of different neuroblast complements in each hemisphere (Figure 1B).

145 Together, these neuroblast losses could potentially produce 10 states for each mushroom body:
146 KCs could be derived from 0-4 neuroblasts, and PNs from 1-2 neuroblasts. Using our reporters,
147 we scored the presence or absence of PNs derived from lNB/BAlc (ventrolateral to the adult an-
148 tennal lobe) and counted the number of KCs (Figure 1C). In practice, some of the 10 states did
149 not occur and some were overrepresented (Figure S2A). Hemispheres from the same brain did
150 not generally show the same neuroblast state as one another, but were often similar in severity
151 of neuroblast losses (Figure S2B).
152
153 KCs of different types are produced in a characteristic sequence in development: γ KCs are
154 born in the embryo and early larva, α'β' KCs are born in late larvae, and αβ KCs are born in pu-
155 pae. We identified samples in which all 4 KC neuroblasts had been ablated by looking for sam-
156 ples lacking mushroom body vertical lobes, which are composed of axons of α'β' and αβ KCs
157 and thus do not form if all KC neuroblasts are killed by HU just after embryo hatching. We con-
158 firmed previous findings that in animals with all four KC neuroblasts ablated, the PNs fail to tar-
159 get the calyx and project only to the lateral horn (Stocker et al., 1997). In these animals, ~100
160 KCs remained (Figure 1B). These represent the KC population that is born prior to larval hatch-
161 ing, and which is thus unaffected by KC neuroblast ablation after hatching. Recently, these earli-
162 est-born cells, called γd KCs, have been shown to receive visual and not olfactory input in adult
163 flies (Vogt et al., 2016; Yagi et al., 2016). These observations suggest that γd KCs are molecu-
164 larly distinct from later-born cells during pupal calyx wiring, such that even when all the olfactory
165 KCs are absent, olfactory PNs cannot innervate visual KCs. Remarkably, these embryonic-born
166 γd KCs receive olfactory inputs in the early larva and are sufficient for olfactory learning at that
167 time (Eichler et al., 2017; Pauls et al., 2010); they must therefore switch their partner prefer-
168 ences across developmental stages.
169

170 We then examined calyx anatomy in animals with intermediate populations of KCs, likely de-
171 rived from 1-3 remaining neuroblasts. We found a progressive decrease in the size of the mush-
172 room body calyx in these animals (Figure 1B, C). To ask if this corresponded to a decline in
173 bouton number, we counted the number of PN boutons in each hemisphere (Figure 1E). This
174 revealed a roughly linear relationship between KC number and PN bouton number, suggesting
175 that PNs reduce their population of boutons to match the KC population. The lateral horn ap-
176 peared normal in these animals and its size did not correlate with KC number, suggesting that
177 PN projections to these two brain areas develop independent of one another (Figure 1B, D).
178 The presence or absence of ventrolateral PNs did not obviously predict bouton number, sug-
179 gesting individual PNs may be able to tailor their bouton production both to the number of KCs
180 and to adjust to the number of other PNs. However, we were not able to obtain enough samples
181 to draw firm conclusions about whether PN cell number affected PN bouton number in calyces
182 derived from matched KC neuroblast complements. To test this, we developed alternative meth-
183 ods to ablate PNs (Figure 5, 6).
184

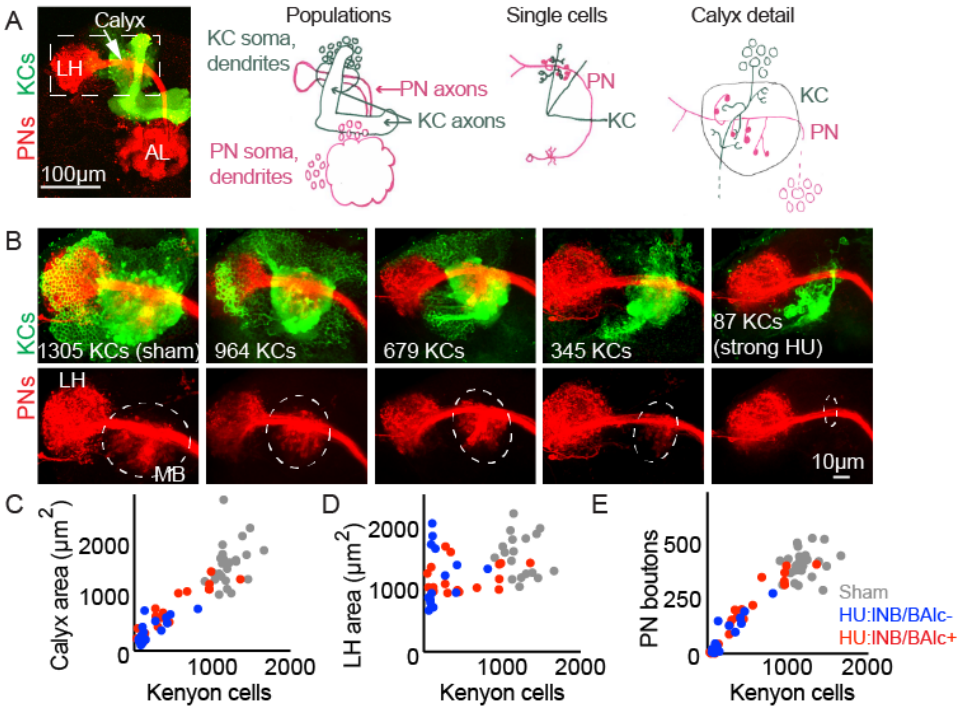

Figure 1: Reduction of Kenyon cells leads to reduced projection neuron innervation of the mushroom body calyx. (A) Images (left) and models (right) of olfactory PNs and KCs in the adult fly brain. PNs (red) receive input from olfactory sensory neurons in the antennal lobe (AL) and project to the mushroom body calyx and the lateral horn (LH). In the calyx, PNs synapse with KCs (green) in microglomeruli. Dashed box at left indicates region shown in B. (B) Maximum intensity projections of confocal stacks of the brains of adult flies subjected to HU treatment or sham treatment just after larval hatching. PNs labeled red using GH146-Gal4, KCs green using MB247-LexA. Dashed ovals indicate the extent of the MB calyx in each sample. (C, D) Relationship between number of KCs and maximum calyx (C) or lateral horn (D) cross-sectional area in HU treated (blue, red dots) and sham treated (grey dots) MBs. Treated samples are separated by presence (red) or absence (blue) of lNB/BAlc progeny. Here and throughout, each dot is one hemisphere. (E) Relationship between KC number and GH146+ bouton number in brains of HU and sham-treated animals.

To score KC clones directly, we developed a strategy to label only the latest-born, "αβ core" KCs. The somata and principle neurites of these late-born cells remain clustered in the adult, allowing us to count KC clones by counting groups of labeled soma or axon tracts as they leave the calyx (Figure 2A, B). Again, we found that calyx size tracked KC clone number, and that the presence or absence of the PN progeny of lNB/BAlc did not predict calyx size (Figure 2C). KC loss could reduce PN bouton number if PNs die or fail to be born when lacking KC contacts or trophic support. We thus counted the number of anterodorsal PNs (derived from adNB/BAmv3)

207 and ventrolateral PNs (derived from lNB/BAlc) in this cohort. The number of anterodorsal PNs
208 was not reduced in animals with some or all KC neuroblasts ablated, and the number of ven-
209 trolateral PNs was binary rather than graded, suggesting that vlPN number is determined by
210 whether lNB/BAlc succumbed to HU, rather than by the KC complement (Figure 2D, E). These
211 results suggest that PN neurogenesis and survival do not require KC signals.
212
213 Reduction in the number of PN boutons in the calyx could occur because individual PNs quanti-
214 tatively reduce their bouton production. To ask whether individual PNs alter their production of
215 presynaptic boutons as the KC repertoire changes, we identified two methods to label single
216 PNs. We focused on anterodorsal PNs, as these are not susceptible to ablation of lNB/BAlc.
217 First, we used 71D09 Gal4 to label the anterodorsal VM6 PN (Ward et al., 2015) and then sub-
218 jected labeled animals to HU ablation. Because we found a linear relationship between KC num-
219 ber and calyx size and between KC clone number and calyx size (Figure 1C, 2C), we used ca-
220 lyx size to infer KC neuroblast status (see methods and Figure S2G). While VM6 usually pro-
221 duces ~10 boutons, we found only ~5 boutons in animals with KCs derived from 1-2 neuro-
222 blasts, and 0-1 bouton in animals with all KC neuroblasts ablated (Figure 2F). These results
223 suggest that individual PNs do reduce their bouton production as the KC complement is re-
224 duced, and that this reduction is graded rather than binary (i.e. in animals with some but not all
225 KC neuroblasts ablated, bouton number is in between 0 and the wild type number). To charac-
226 terize additional PNs, we expressed photoactivatable GFP under control of R42D01-Gal4, which
227 labels ~10 anterodorsal PNs innervating the VM3 and VM4 glomeruli. We photoconverted indi-
228 vidual somata using two photon microscopy. Though bouton counts were somewhat more varia-
229 ble than for VM6 as this strategy labels different types of PNs with different characteristic bouton
230 numbers, we again found a correlation between KC neuroblast number and bouton number
231 (Figure 2G).
232

233 The linear reductions in bouton number we observed for different PN types would preserve the
234 relative representation of these odor channels in the calyx. While the genetic constraints of
235 these experiments prevented us from scoring the status of lNB/BAlc, we also note that the
236 range of bouton numbers we observed are consistent with adjustments to compensate for the
237 presence or absence of ventrolateral PNs. For example, most VM6 neurons innervating a calyx
238 derived from 1 KC neuroblast produced between 3 and 7 boutons, as compared to the median
239 of 10 in unperturbed animals. If KCs are reduced by ¾ without loss of lNB/BAlc, perfect com-
240 pensation by PNs would reduce boutons from 10 to 2.5. If lNB/BAlc was also lost, perfect com-
241 pensation would reduce boutons from 10 to 5. These predicted values are similar to the bouton
242 range we observed experimentally.
243
244 Finally, we sought to ask if KC claw number changes as KC number changes. We used GFP
245 photoactivation to label individual KCs in animals subjected to HU ablation. The different KC
246 classes have different median claw numbers: γ KCs have ~7 claws, αβ cells have ~5 claws, and
247 α'β' KCs have ~3 claws; we therefore analyzed KC types separately. For both αβ and γ KCs, we
248 found no change in claw number on individual KCs as the KC population was reduced (Figure
249 2H, I). From these experiments, we conclude that PNs reduce their bouton production on a cell-
250 by-cell basis as the KC population shrinks, while KC claw number is unaffected by the size of
251 the KC population (model, Figure 2J).
252

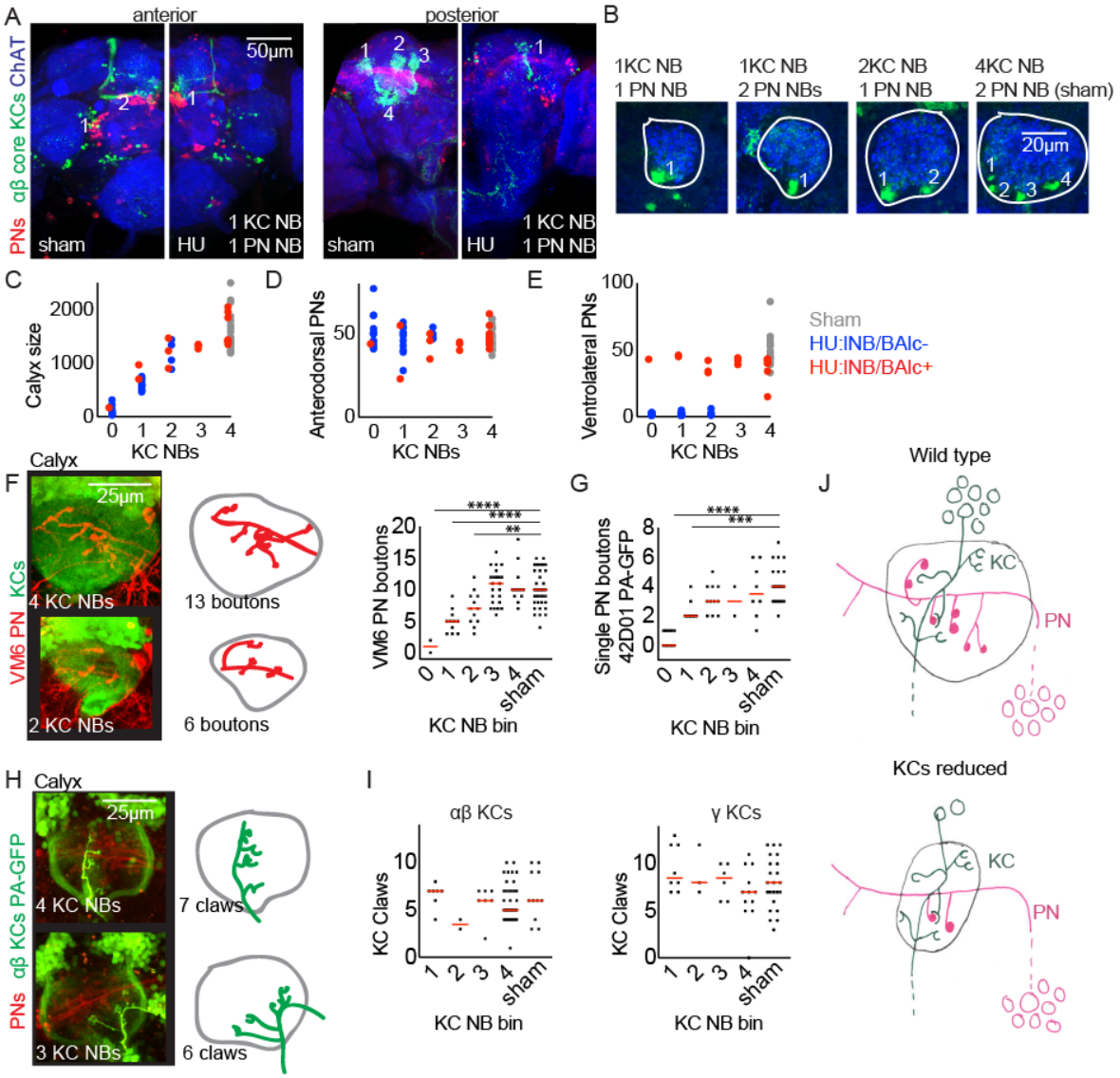

Figure 2: Individual projection neurons scale their bouton repertoire to the Kenyon cell population. (A) Maximum intensity projections of confocal stacks of the anterior (left) and posterior (right) of HU and sham-treated animals. GH146 labels PNs (red). 58F02 labels late-born αβ "core" KCs (green). Cholinergic neurons labeled with ChAT immunostaining (blue). Numbers indicate PN and KC clones. Anterior and posterior images are of the same brains. (B) Confocal slices of the mushroom body calyx in sham-treated (right) and various HU treated (left) hemispheres. ChAT signal highlights bouton structures, while 58F02 signal allows scoring of the number of KC clones. (C-E) Relationship between KC clone number and maximum calyx cross-sectional area (C), and number of anterodorsal (D) and ventrolateral (E) PNs. (F) Example images and diagrams (left) and quantification (right) of MB calyx boutons on the VM6 PN, labeled by 71D09 (red). KCs labeled by MB247 (green). Examples show two hemispheres of the same brain of a HU treated animal, with the extent of the calyx shown in grey. Neuroblast bin was determined by calyx size, as described in the methods. Significance, unpaired t-tests of each HU treated KC neuroblast bin to sham corrected for multiple comparisons. Comparisons not indicated are not significant. Here and throughout, horizontal bars reflect medians; *: $\rho<0.05$, **:

269 $\rho<0.01$, ***: $\rho<0.001$, ****: $\rho<0.0001$. (G) Quantitation as described in (F) of single PNs within
270 the 42D01-Gal4 expression pattern highlighted by GFP photoactivation. (H, I) GFP photoactiva-
271 tion of individual KCs in HU treated or sham brains. Example and diagrams in (H) show two
272 hemispheres of the same HU treated brain of an animal with PNs labeled by 60A10 and $\alpha\beta$
273 "core" KCs by 58F02. lNB/BAlc status was recorded and is shown in Figure S2C-F. (J) Model of
274 the effect of KC loss on calyx development. Remaining KCs exhibit wild-type numbers of claws,
275 while PNs reduce their bouton repertoire, reducing the size of the calyx.
276

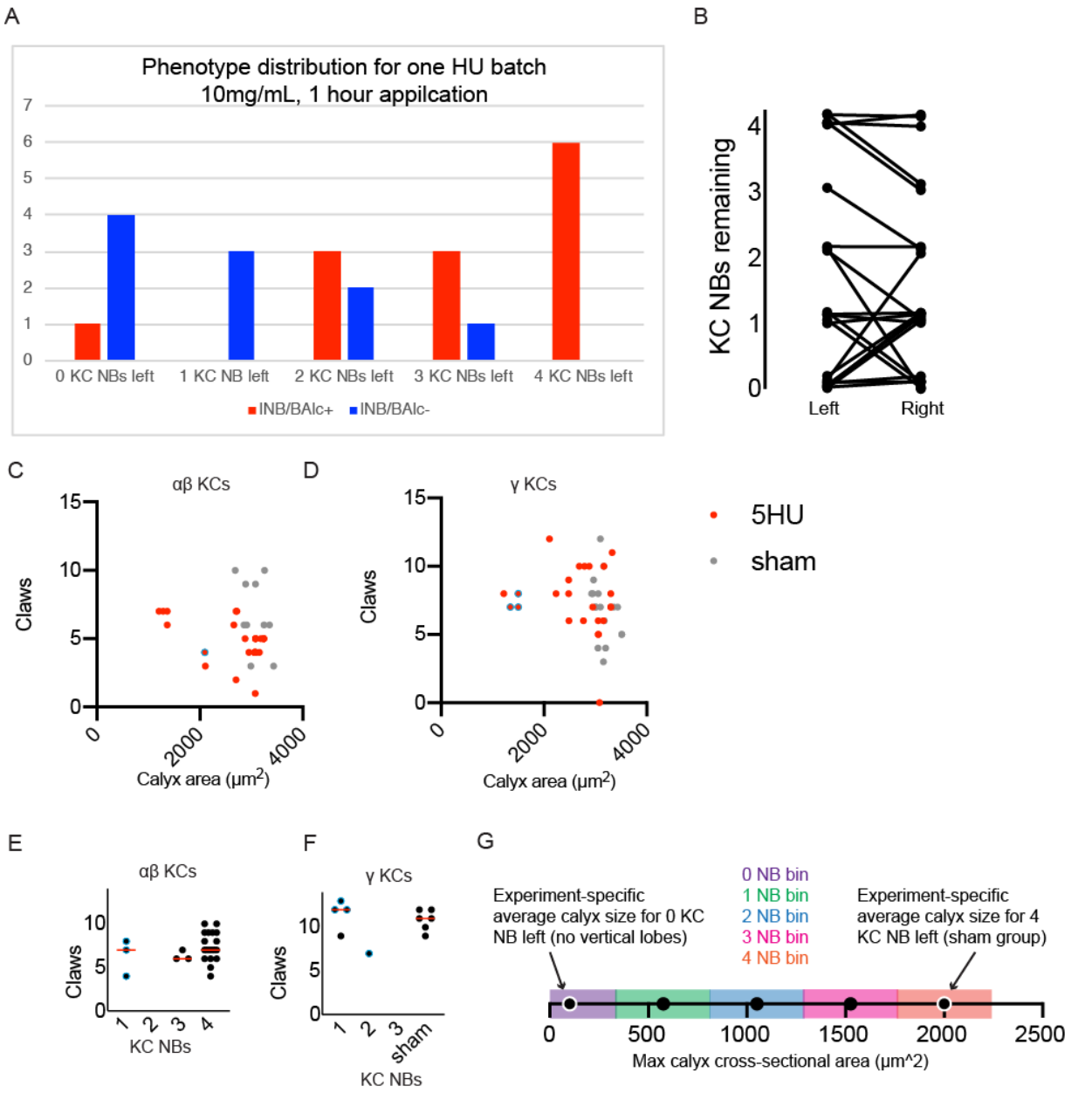

Figure S2: Supplemental data related to Figure 2. (A) Distribution of HU effects for one batch of treated animals. Genotype as in Figure 2A. (B) Relationship of KC neuroblast state across hemispheres. Jitter was added to make each sample apparent. (C-F) Disaggregated data for KC claw quantification shown in Figure 2I. In S2C, D, MB247 was used to drive PA-GFP expression in all KCs, KC type was defined by tracing axonal projections, and KC neuroblast status was inferred from calyx size. In E, F KCs of a single type were labeled with PA-GFP, and KC neuroblast status was inferred directly from KC labeling patterns. Samples in which INB/BAlc was not present are circled in blue. (G) Calculation for inferring KC neuroblast number from calyx size based on the linear relationship observed in Figures 1C, 2C. Calyx size for true 0-neuroblast and 4-neuroblast samples were experimentally measured and expected calyx size bins for calyces derived from 1-3 KC neuroblasts were computationally interpolated between them.

290 **Olfactory projection neurons increase bouton repertoire as Kenyon cell number in-**
291 **creases**
292 In order to assess whether PNs can vary their presynaptic bouton number bidirectionally, we
293 next created a method to specifically amplify the KC population. Recent work has suggested
294 that ectopic or supernumary populations of neurons can integrate into a variety of fruit fly neural
295 circuits (Pop et al., 2019; Prieto-Godino et al., 2019; Shaw et al., 2018), and previous studies
296 identified a mutant, called *mushroom body defect* (*mud*) in which the mushroom body and other
297 brain areas are dramatically expanded (Guan et al., 2000; Prokop and Technau, 1994).
298 Mud/NuMA is a spindle orientation protein that ensures neuroblasts divide asymmetrically to
299 produce one neuroblast and one differentiating neuron or neural progenitor (Siller et al., 2006).
300 In *mud* mutants, neuroblasts occasionally divide symmetrically to produce two neuroblasts, am-
301 plifying the progeny of that neuroblast. To restrict amplification to KC neuroblasts, we drove
302 UAS-*mud*-RNAi (BL 35044) in KC neuroblasts using OK107-Gal4 (Liu et al., 2015). As OK107
303 labels mature KCs as well as KC neuroblasts, we included UAS-CD8GFP in these animals to
304 count KCs. This produced potent amplification of KCs that was variable across animals, some-
305 times more than doubling KC number (Figure 3A, B). We measured calyx size, which expanded
306 dramatically, and used ChAT immunoreactivity to count PN bouton number, which doubled in
307 mushroom bodies with the largest KC expansions (Figure 3B). These results suggest that just
308 as PNs scale down their boutons if the KC population is reduced, PNs scale up their boutons
309 when the KC population is expanded.
310
311 To test whether PNs increased boutons on a cell-by-cell basis in these animals, we labeled VM6
312 using 71D09-LexA, and PNs innervating DA1, Va1d, and DC3 using MZ19-QF. First, we ob-
313 served no change in VM6 or MZ19+ cell numbers in brains with KCs expansions, suggesting
314 that PN numbers do not increase as KC number increases. We observed no change in VM6
315 bouton numbers, perhaps because the VM6 PN already has a relatively large number of

316 boutons (Figure S3A). In contrast, MZ19 cells increased their number of presynaptic boutons as
317 the KC population expanded, from an average of 3.5 boutons per cells in the control genotype
318 to an average of 4.75 boutons per cell in the KC-expansion genotype. In the brains with the larg-
319 est KC expansions, MZ19+ boutons doubled (Figure 3C-D).
320
321 To rule out reductions in the number of claws per KC as the KC population expands, we ex-
322 pressed photoactivatable GFP under the control of OK107 in animals with UAS-*mud*-RNAi or
323 control and subjected individual or small groups of KCs to photoactivation. We scored the num-
324 ber of claws per labeled KC in each calyx. As above, calyx size predicted KC number in these
325 animals, so we used calyx size as a proxy for KC number. Rather than a decrease in claw num-
326 ber per KC in animals with expanded KC complements, we found a slight increase in claw num-
327 ber, from a median of 5 to a median of 6 claws. As different types of KCs produce different char-
328 acteristic numbers of claws, this could represent a change in claw production, a change in the
329 distribution of KC types in these animals, or bias in which KC types we labeled in expanded vs
330 control brains. While we were unable to identify LexA lines to specifically label $\alpha\beta$ or γ KCs in
331 OK107->mudRNAi brains, we found a LexA line, R41C07, that labeled $\alpha'\beta'$ KCs, and targeted
332 these specifically for photoactivation (Figure S3B). In these KCs of matched type, we found no
333 change in KC claw number per cell, though we cannot rule out subtle differences. Together,
334 these experiments suggest that in animals with an amplified KC complement, PNs dramatically
335 increase their bouton production to match the KC population, while KCs may moderately in-
336 crease, and do not reduce, their individual claw production.
337

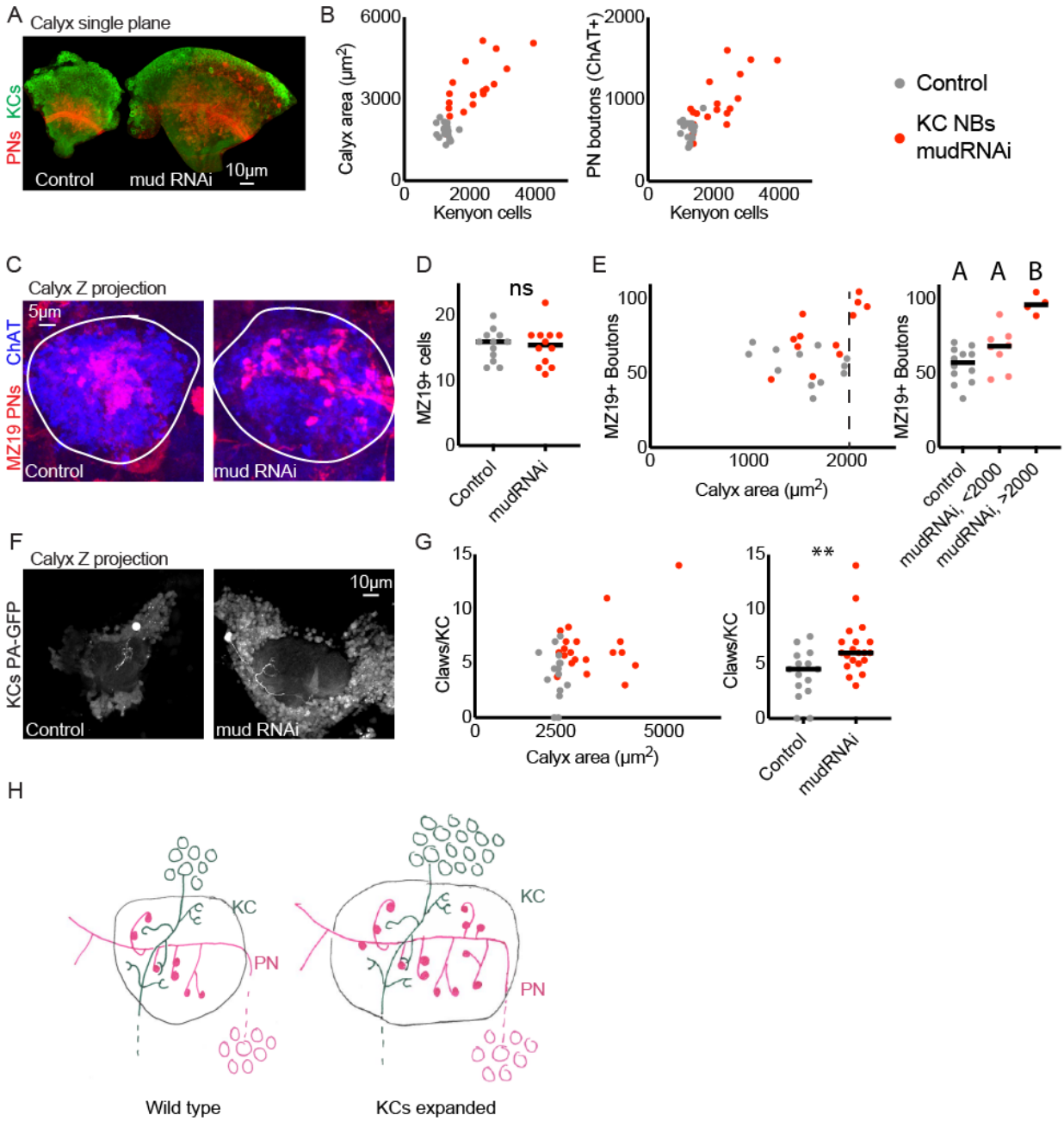

Figure 3: Increase in Kenyon cell number leads to increased projection neuron bouton complement. (A) Confocal slice of control calyx and calyx subjected to KC expansion by expression of *mud*-RNAi in KC neuroblasts via OK107-Gal4. GH146 labels PNs (red) and OK107 labels KCs (green). (B) Relationship between number of KCs and maximum calyx cross-sectional area (left) and PN bouton number (right) in control (grey) and KC neuroblast->mud-RNAi hemispheres (red). (C) Maximum intensity projection of confocal stack of calyx bouton production by ~16 MZ19+ PNs (red) in control and KC neuroblast->mud-RNAi. ChAT immunostaining (blue) highlights calyx extent. (D) Quantification of MZ19 cells in the two genotypes. Significance: unpaired t-test. (E) Relationship between maximum calyx cross-sectional area (a proxy for KC number) and MZ19 bouton production. Vertical dashed line indicates 2000 μm^2, as calyces larger than this were observed only in the experimental genotype. Significance: one-way

ANOVA. (F) Maximum intensity projection of two-photon stack of single KCs highlighted by GFP photoactivation (C3PA driven by OK107) in control or KC neuroblast->mudRNAi calyces. Position of out-of-plane somata in control image indicated by white circle. (G) Quantification of claws of KCs labeled as in (F). Y axis is average number of claws per KC as multiple KCs were photoactivated in some samples. Significance: unpaired t-test. (H) Model of the effect of KC expansion on calyx development. KCs retain normal claw numbers while PNs increase their bouton numbers, increasing calyx size.

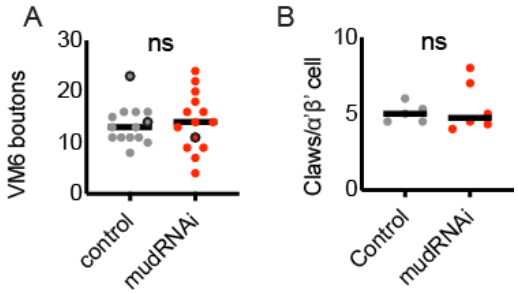

Figure S3. Supplemental data related to Figure 4. (A) Boutons of the VM6 PN in control (grey) or brains subjected to KC expansion via OK107->mudRNAi (red) . Every hemisphere contained one VM6 neuron in both genotypes except the three circled datapoints, which had two VM6 PNs. Significance: unpaired t-test. (B) KC claw number in PA-GFP-labeled α'β' KCs in control or KC-expansion genotype. Significance: unpaired t-test.

Individual projection neurons decrease bouton number as the projection neuron population expands

We have shown that olfactory PNs bidirectionally vary their presynaptic boutons to suit populations of KCs derived from 0-8 KC neuroblasts. To ask whether PNs can also vary their bouton production in response to changes in their own numbers, or in response to changes in the ratio between PNs and KCs that do not affect KC clone number, we identified methods to vary the PN population. We found that just as we could expand the KC population by knocking down *mud* in KC neuroblasts, we could expand the PN population by knocking down *mud* in PN neuroblasts. This strategy produced PN complements of up to 600 cells, as compared to 150 cells in the control. While the PN neuroblast Gal4 we used, 44F03, can label both lNB/BAlc and adNB/BAmv3 progeny (Awasaki et al., 2014), we found that ventrolateral PNs were much more susceptible to expansion than anterodorsal PNs.

381 Supernumary PNs innervated the antennal lobe, causing a massive expansion of antennal lobe
382 area (Figure 4A, B). The normal glomerular map in the AL appeared distorted, but glomerular
383 divisions were still present. These PNs also projected to the calyx, observed by thickening of the
384 PN axon tract entering and crossing the calyx, and increased the density of PN innervation of
385 the lateral horn (Figure 4C), though not lateral horn area (Figure S4A). However, there was no
386 change in calyx area or total bouton number in these animals compared to wild type (Figure 4D,
387 E). At a population level, the average number of boutons per PN was half that in controls (Fig-
388 ure 4F).
389
390 To ask how small groups of PNs adjusted to PN expansion, we again used MZ19-QF, which la-
391 bels 15-20 PNs in controls (Figure 4G, H). We counted MZ19+ cells and boutons in control ver-
392 sus animals of the expansion genotype (Figure 4H). As the expansion was highly variable and
393 we rarely observed more than 25 MZ19+ cells in controls, we divided the expanded genotype
394 into hemispheres with <25 PNs or >=25 PNs. There was a modest but insignificant increase in
395 MZ19+ boutons in the >=25 PNs groups (Figure 4H), attributable to a strong and significant re-
396 duction of average number of boutons per PN (Figure 4H). Thus PNs scale down their individual
397 bouton repertoire to compensate for increases in the size of the PN population. Like MZ19 PNs,
398 the VM6 PN also maintained a stable number of total boutons as the PN population expanded
399 (Figure S4A). This was possible because the VM6 cell(s) had similar numbers of total boutons
400 as the VM6 population expanded.

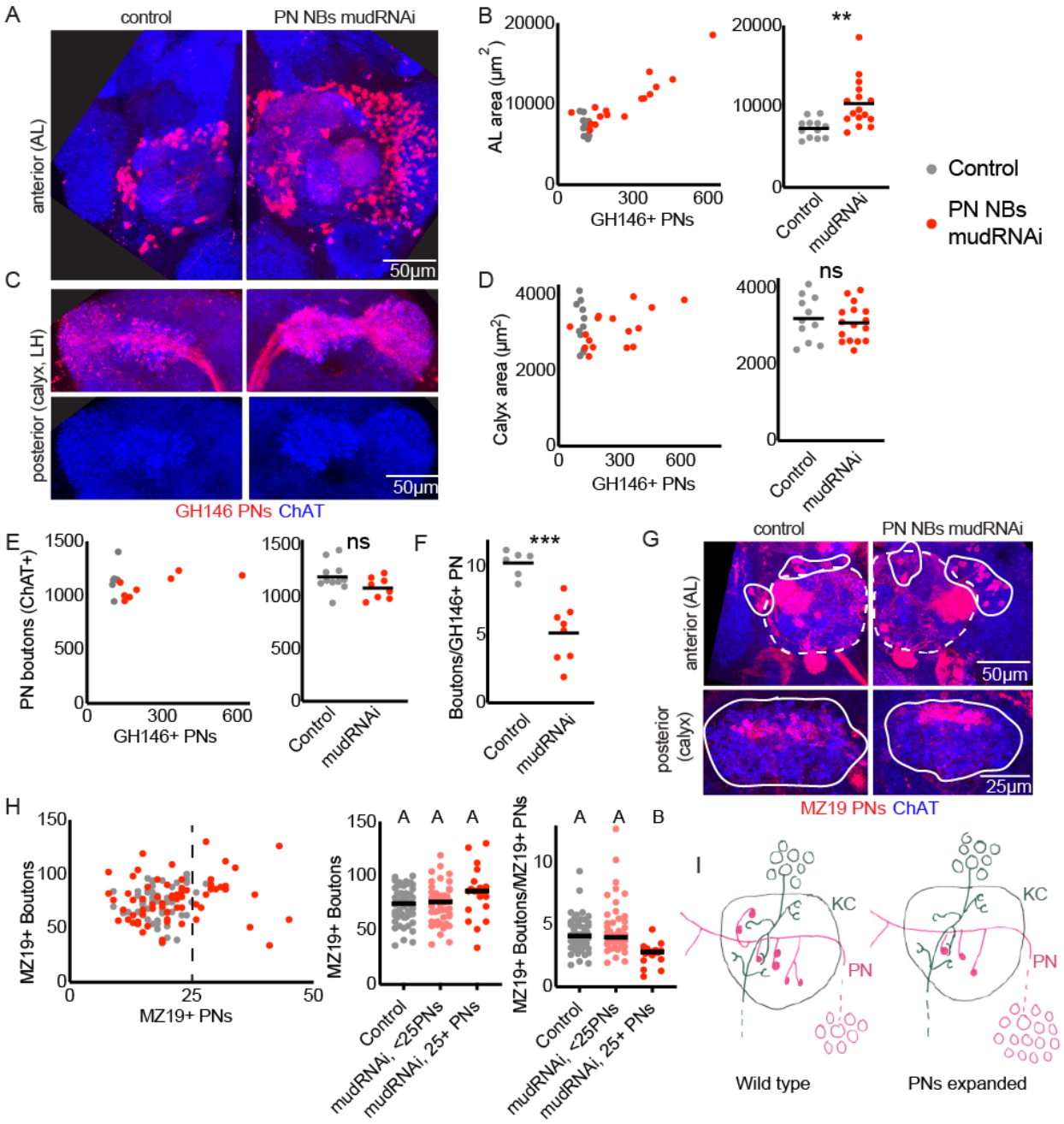

Figure 4: Individual projection neurons scale boutons down as projection neuron population increases. (A) Maximum intensity projection of confocal stack of anterior of the brain of control subjected to PN expansion by expression of *mud*-RNAi in PN neuroblasts via 44F03-Gal4. GH146 labels PNs (red) and ChAT staining highlights cholinergic neurons. (B) Relationship between PN number (measured by counting GH146+ cells, about 60% of the total PNs) and antennal lobe maximum cross-sectional area in control (grey) or PN neuroblast->mudRNAi hemispheres (red). Significance: unpaired t-test. (C) Maximum intensity projection of confocal stacks of the posteriors of the same brains shown in A. Excess PNs can be seen to project to the calyx, due to thickening of the axonal tract entering and crossing the calyx, and produce increased innervation density in the lateral horn. (D-F) Relationship between PN number and maximum cross-sectional area of the calyx (D), PN bouton number (E), and ratio of ChAT+-

413 boutons to GH146+ PNs (F) in control and PN neuroblast->mudRNAi brains. Significance: un-
414 paired t-test. (G) Maximum-intensity projections of confocal stacks of antennal lobes (top) and
415 calyces (bottom) of control and PN neuroblast->mudRNAi brains. MZ19+ PNs labeled red.
416 Dashed outlines on anterior show antennal lobe extent; solid outline on anterior, groups of PN
417 somata; solid outlines on posterior, calyx extent. (H) Quantification of MZ19+ boutons in control
418 and PN neuroblast->mudRNAi brains. Dashed horizontal line indicated 25 MZ19+ PNs, as con-
419 trols seldom exceed this number. Significance: one-way ANOVA. (I) Model of the effect of in-
420 creasing PN numbers on calyx development. As PNs increase, PNs reduce bouton production
421 so that the overall number of boutons, and calyx size, stays similar to wild type.
422

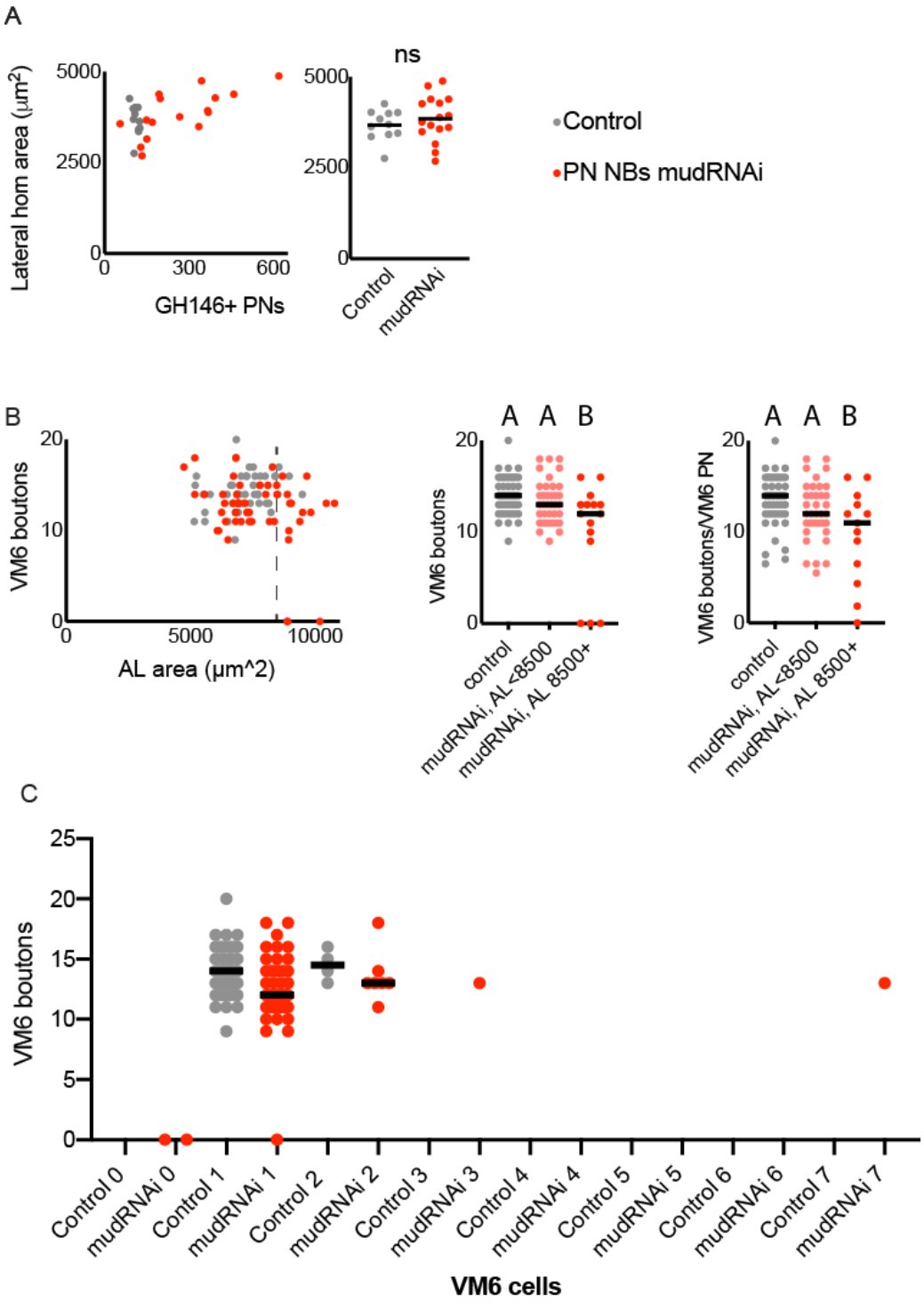

Figure S4: Supplemental data related to Figure 4. (A) Relationship between lateral horn maximum cross-sectional area and PN number in control (grey) and PN neuroblast->mudRNAi (red) brains. Significance: unpaired t-test. (B) Relationship between antennal lobe maximum cross-sectional area (proxy for PN number) and production of calyx boutons by the VM6 PN, labeled by 71D09. Dashed line indicates 8500 μm^2, as antennal lobes larger than this were observed rarely in the control genotype. Significance: one-way ANOVA. In two experimental hemispheres,

430 we observed no VM6 PN. In one hemisphere, we observed one VM6 PN with no boutons in the
431 calyx. (C) VM6 boutons in calyces of brains containing different numbers of VM6 PNs. We ob-
432 served more than one VM6 PN in 4/50 control and 9/50 PN neuroblast->mudRNAi hemi-
433 spheres.
434

435 **Projection neurons bouton expansion partially compensates for severe reductions in the**
436 **projection neuron population**

437 In order to reduce the PN repertoire independent of KC number, we identified two Gal4 lines,
438 VT033006 and VT033008, that label large PN complements in the adult (Figure 5A). We drove
439 diphtheria toxin A (Berdnik et al., 2006) and fluorescent reporters under control of these lines in
440 animals where additional PNs were labeled by GH146-LexA (Figure 5B, F). In each case, DTA
441 eliminated all Gal4+ cells as well as additional GH146+ PNs, suggesting that these lines drive
442 DTA expression in broader PN populations at earlier stages of development. Driving DTA under
443 control of VT033008 reduced the total PNs labeled by VT033008 and/or GH146 by nearly half
444 (Figure 5C), while VT033006->DTA reduced PNs labeled by VT03006 and/or GH146 by >90%
445 (Figure 5G). While PN dendrites have been shown to occupy glomerular territories in pupal
446 stages before OSNs innervate the antennal lobe (Jefferis et al., 2004), we found that antennal
447 lobes lacking the vast majority of uniglomerular PNs retained glomerular divisions. This sug-
448 gests that PNs may not be required for the formation of glomerular divisions in the adult anten-
449 nal lobe.
450

451 We measured calyx size and bouton number across these conditions and found that in each
452 case, the effect on the calyx was measurable but much less severe than the reduction in PN
453 number. For VT033008->DTA, loss of nearly half the PNs yielded no change in calyx size and a
454 20% reduction in overall bouton number (Figure 5D, E). Remarkably, while we estimate that
455 only ~10 PNs remain in VT033006->DTA animals (~5% the normal complement), the number of
456 boutons in the calyx was reduced by only half (Figure 5H, J). This suggests that individual PNs
457 could have expanded their bouton production by as much as 6-fold. While remaining PNs

458 sometimes appeared to make exuberant collections of boutons (e.g. Figure 6C), distortion of the
459 antennal lobes in these animals prevented us from assigning identities to these spared PNs and
460 comparing bouton numbers to matched individual PNs in controls.
461
462 This severe loss of inputs could lead to KC death. We therefore labeled and counted KCs in
463 VT033006->DTA animals with severe PN loss. While we cannot rule out a small reduction in KC
464 complement, at least 80% of KCs survived in these brains. We also subjected control and
465 VT033006->DTA brains to flow cytometry and found that PN ablation brains had at least 85% as
466 many KCs as did control brains (Figure S5).
467

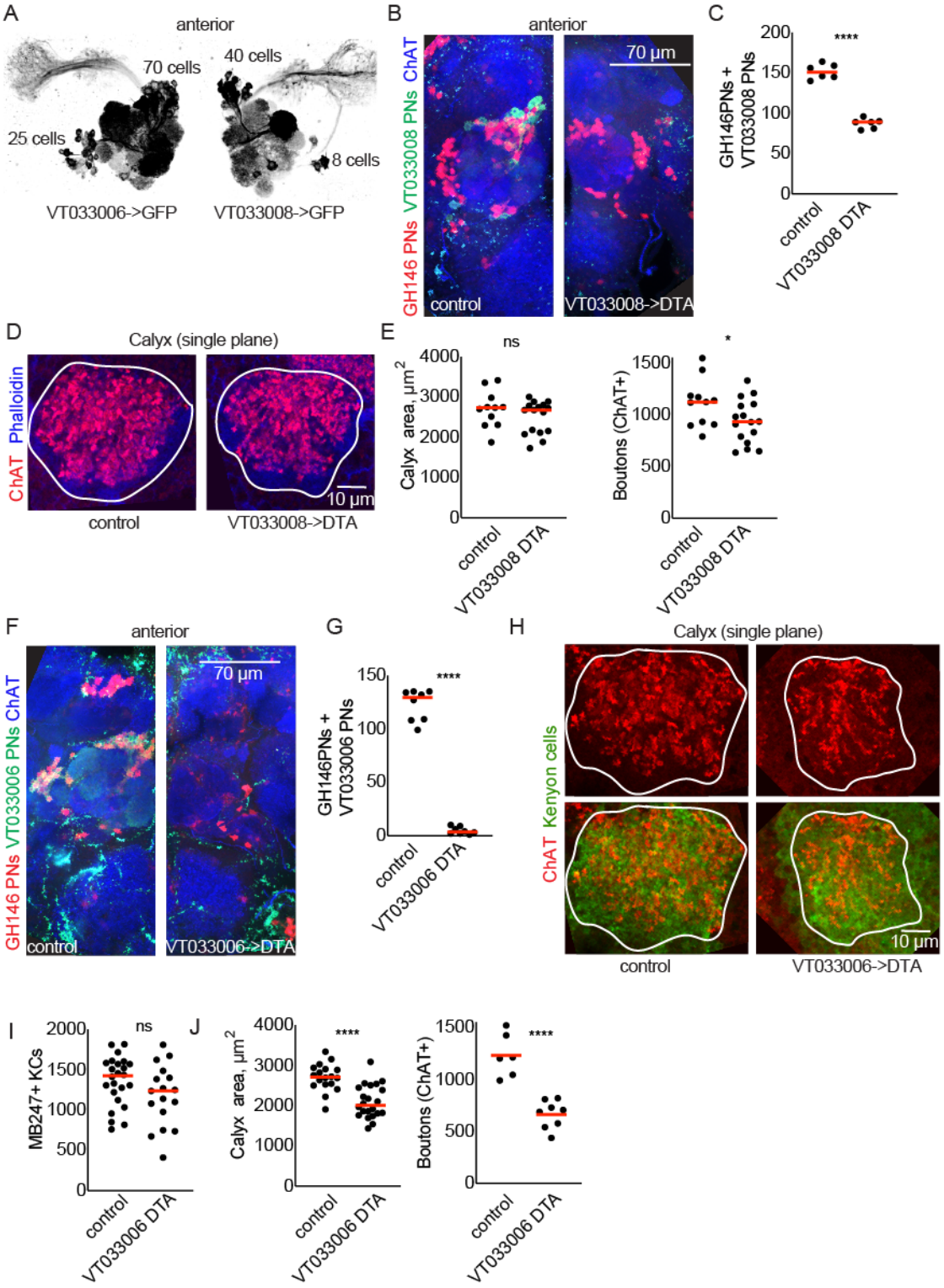

Figure 5: Projection neurons partially compensate for decreases in projection neuron population. (A) Maximum-intensity projections of two-photon stacks of brains with VT033006 (left) and VT033008 (right) driving GFP. (B) Maximum intensity projection of confocal stack of antennal lobes of control (left) and VT033008->DTA (right) brains. VT033008+ cells shown in

green, GH146+ PNs, which partially overlap with VT033008+ PNs, shown in red. (C) Quantitation of PNs positive for GH146, VT033008, or both in control and VT033008->DTA brains. All VT033008+ cells are ablated in this genotype. Significance: unpaired t-test. (D) Single confocal slice of control or VT033008->DTA calyx. Phalloidin signal shown in blue and ChAT+-boutons shown in red. (E) Quantification of calyx maximum cross-sectional area and bouton number in control and VT033008->DTA animals. Significance: unpaired t-test. (F) Maximum intensity projection of confocal stack of antennal lobes of control (left) and VT033006->DTA (right) brains. VT033006+ cells shown in green, GH146+ PNs, which partially overlap with VT033006+ PNs, shown in red. (G) Quantitation of PNs positive for GH146, VT033006, or both in control and VT033006->DTA brains. All VT033006+ cells are ablated in this genotype as well as most GH146+ PNs, even those that are not VT033006+ in the adult. Examination of ChAT+ neurites entering the calyx in VT033006->DTA brains suggests that up to 10 PNs may be labeled by neither VT033006 nor GH146, and that some of these may survive ablation. Significance: unpaired t-test. (H) Single confocal slice of control (left) or VT033006->DTA (right) calyx. KCs labeled green using MB247, ChAT+ boutons shown in red. (I) Quantification of the number of MB247+ KCs in control or VT033006->DTA brains. Significance: unpaired t-test. (J) Quantification of calyx area and ChAT+ boutons in control or VT033006->DTA brains. Significance: unpaired t-test.

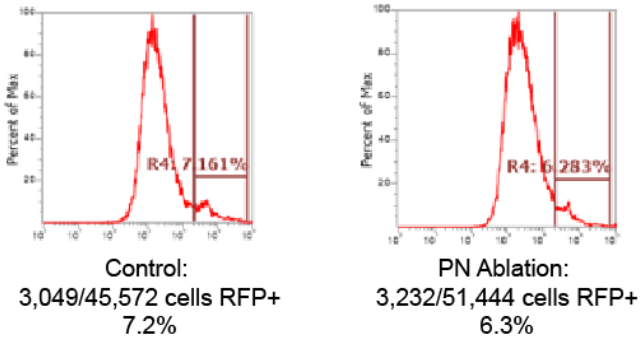

Figure S5: Data related to Figure 5. Number of KCs (MB247-dsRed, RFP+) detected in 3 pooled control or 3 pooled VT033006->DTA brains dissociated and subjected to flow cytometry. Plots depict cells already gated as singlets positive for a DNA dye, dyeCycle Violet. Representative of two experiments.

Projection neuron insufficiency has little effect on Kenyon cell claw number

We expected that while KC claw number was largely invariant in the face of increases and decreases of the KC population, KCs would be forced to reduce their claw number when PN bouton production was reduced by 50%, as in VT033006->DTA animals. We therefore compared individual KCs in these animals versus controls. As different KC types produce different numbers of claws in wild type, we sought to simplify the analysis by labeling only a single KC type. To do this, we targeted Texas red dextran dye electroporation to the tips of the mushroom body

504 α lobes, which are innervated by αβ KCs (Figure 6A). This allowed us to label 1-12 KCs per ca-
505 lyx. We could discern discrete dye-labeled claws and somata in animals with eight or fewer KCs
506 labeled, and restricted our analyses to these samples (Figure 6 B-D). For each hemisphere we
507 counted labeled somata and claws, generating one average value, claws per labeled KC, per
508 separable group of cells (Figure 6F). Surprisingly, despite 90% reduction in the number of PNs
509 and 50% reduction in their boutons, we observed no reduction in claw number per KC.
510
511 Do these enduring claws receive inputs? While labeled KCs in VT033006->DTA brains some-
512 times made clear contacts with spared PNs, as in Figure 6C, E, in other samples we also ob-
513 served KCs that avoided the one or few GH146-labeled, spared PNs (data not shown). Besides
514 PNs, GH146 labels an inhibitory neuron, APL, that innervates the mushroom body lobes and ca-
515 lyx. APL is presynaptic to KCs in the calyx, but innervates portions of KCs that are not claws
516 (Lin et al., 2014; Zheng et al., 2018). Labeled KCs in VT033006->DTA brains still formed con-
517 tacts with APL (Figure 6D). Alternatively or in addition, 10% of bouton inputs to the main (olfac-
518 tory) calyx are from gustatory or thermal modalities (Caron et al., 2013; Eichler et al., 2017;
519 Kirkhart and Scott, 2015; Zheng et al., 2018). While the neurons bringing this information to the
520 calyx have not been identified, they too could have expanded their production of boutons to
521 make up for the losses of olfactory PNs. We cannot yet determine whether the excess KC claws
522 observed in this condition get inputs from PN boutons, from APL, or from some other source.
523 Nevertheless, these data suggest that KCs are inflexible in their production of claws, even in the
524 face of severe reduction of their typical, favored presynaptic partners.

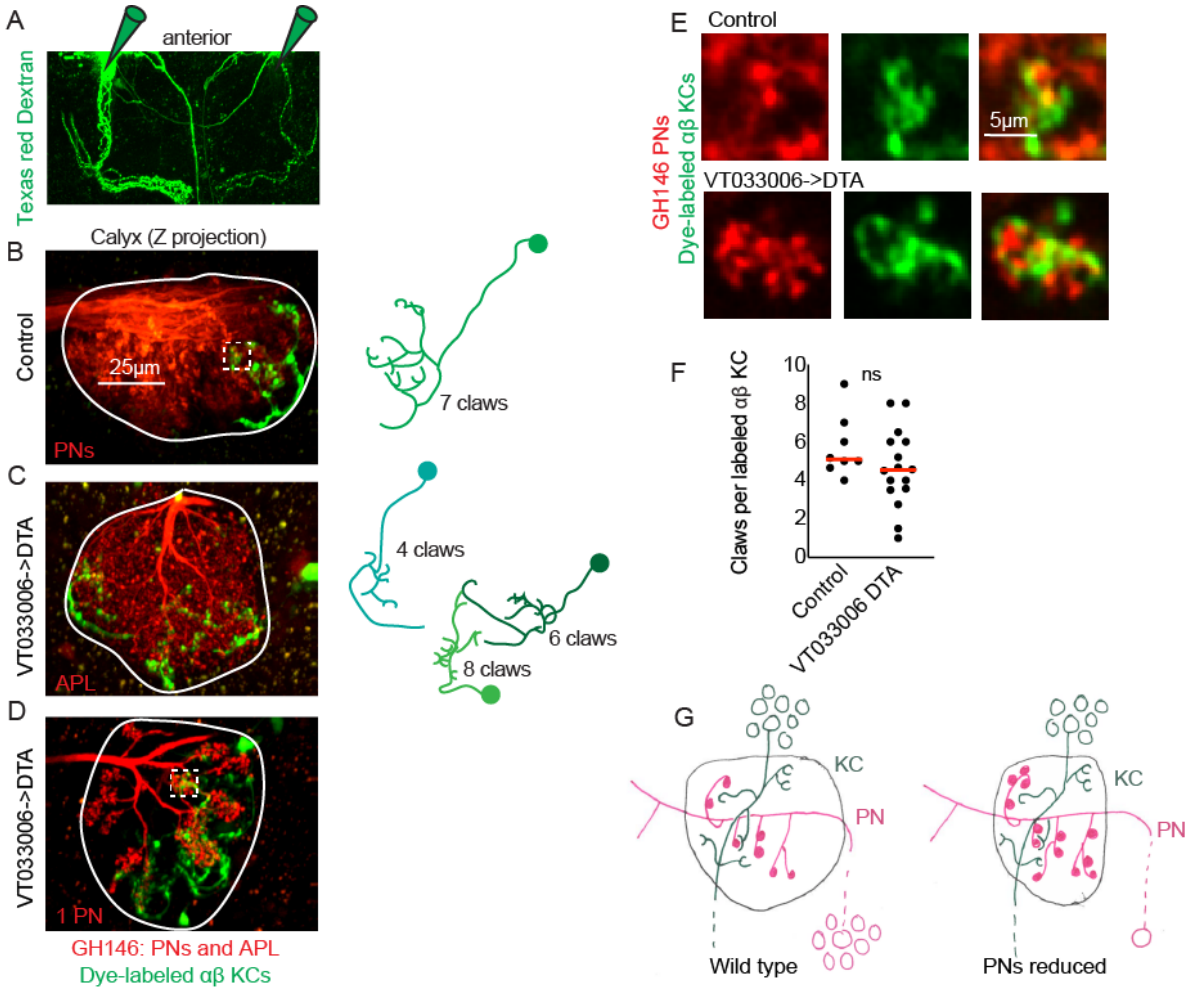

Figure 6: Kenyon cell claw number is unaffected by projection neuron bouton reduction. (A) Texas red dextran (colored green for continuity with green KCs in other figures) was electroporated into the tips of the mushroom body α lobes to allow specific targeting of αβ KCs. (B-D) Maximum intensity two photon stacks of control (B) and VT033006->DTA (C, D) calyces. GH146, shown in red, labels PNs and APL. In control (B), APL is obscured by dense PN signal. In some VT033006->DTA hemispheres, as in (C), all GH146+ PNs were ablated, making APL signal apparent. In other VT033006->DTA hemispheres, as in (D), 1-2 GH146+ PNs remained. Texas red dextran dye diffusing from KC axons is shown in green. Diagrams show reconstructed anatomies of dye-labeled KCs. In (B), one KC with 7 claws is labeled. In C, three KCs with 4, 6, and 8 claws are labeled and can be spatially separated from one another. In D, 8 KCs are labeled and cannot be reconstructed. White boxes in (B) and (D) show regions magnified in (E). (E) Texas red dextran dye-labeled KC claws (green) wrapping GH146+ PN boutons (red) in control (top) and VT033006->DTA brains. (F) Quantification of claws per KC in control or VT033006->DTA samples. Each data point is the average number of claws per labeled KC for a spatially separated individual KC or small group of KCs. Significance: unpaired t-test. (G) Model of the effect on calyx development of ablating large groups of PNs. Remaining PNs increase their production of boutons but cannot fully compensate for lost PNs, reducing the size of the calyx. KC claw numbers are similar to wild type; their source of innervation is unknown.

545 **Developmental plasticity preserves sparse odor coding despite perturbations to cell pop-**
546 **ulations**
547 The disparate and numerous strategies we used above to vary the ratio between PNs and KCs
548 all produced the same result, that PNs adjusted to changes in PN::KC ratio by altering their pre-
549 synaptic boutons, while the distribution of KC claw numbers changed little even when perturba-
550 tions to PNs were so severe as to prevent production of the normal bouton complement. This
551 finding suggests that developmental mechanisms prioritize the sparseness of olfactory inputs to
552 KCs, and might therefore preserve sparse odor coding and high-dimensional odor representa-
553 tions despite stark changes to the underlying circuit constituents. We therefore sought to ask
554 how KC odor responses were affected by perturbations to the PN::KC ratio.
555
556 We used OK107 to drive GCaMP expression in all KCs, and subjected animals to HU just after
557 larval hatching. We then imaged KC somatic odor responses *in vivo* in adult HU or sham-treated
558 animals. Among ablated animals, we identified 3 of 22 hemispheres in which calyces were
559 clearly still present but of reduced size. While we do not attempt to draw fine quantitative com-
560 parisons between reduced-KC and sham-treated animals given the small sample size, we were
561 able to make qualitative assessments of odor responses in these animals.
562
563 We found that KCs in reduced calyces responded to odor. In three HU reduced calyces and
564 sham controls, we identified individual KC somata (22-102 cells/sample) and quantified change
565 in fluorescence to each of four odor stimuli, and in most cases to a mineral oil control (Figure
566 7A, Figure S7). We then set a threshold of 20% increase in fluorescence upon odor stimulation
567 to quantify how many cells responded to each odor; this threshold captured odor-linked re-
568 sponses but not motion-induced shifts in cells across ROI boundaries. Depending on the odor,
569 5-40% of cells passed this threshold in both control and reduced-KC calyces (Figure 7C, D). We
570 observed variation in odor responses in both control and reduced-KC calyces; interindividual

571 variation is expected given the stochastic innervation of KCs by PNs, and the amount of varia-
572 tion we observe is similar to previous reports (Honegger et al., 2011). Importantly, responsive-
573 ness ranges to each individual odor were similar between sham-treated and reduced-KC caly-
574 ces. Finally, we asked how many cells in each sample responded to multiple odors (Figure 7E).
575 In each sample, ~75% of cells responded to 0 or 1 odors, and the proportion of cells responding
576 to multiple odors was similar across conditions. Together, these findings suggest that the devel-
577 opmental plasticity mechanisms operating to set the density of olfactory inputs to KCs preserve
578 qualitatively sparse KC odor responses when the KC population is experimentally reduced.

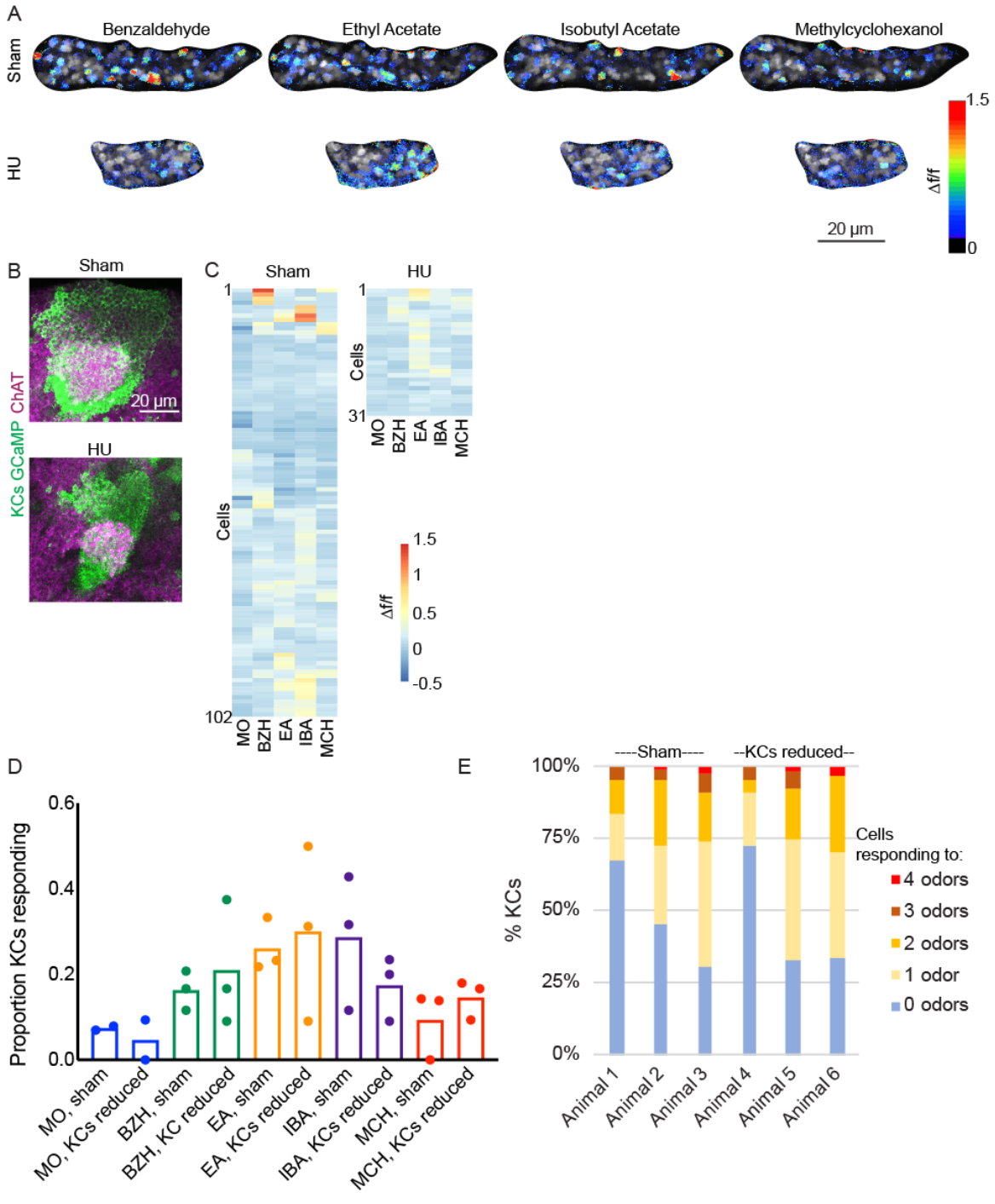

Figure 7: Odor responses in calyces with reduced KCs. (A) Example KC somatic odor responses in sham-treated hemisphere and hemisphere with reduced KCs. (B) Post-imaging immunostaining showing calyces and KC somata of samples shown in (A). (C) Individual odor responses of each KC shown in (A). Data was clustered by row such that cells with more similar odor responses are closer to one another. MO: Mineral oil (mechanosensory control), BZH: Benzaldehyde, EA: Ethyl Acetate, IBA: Isobutyl Acetate, MCH: Methylcyclohexanol. (D) Proportion of cells in each sample with 20% or greater increase in fluorescence intensity in response to

listed odor. (E) Fraction of cells in each sample responding to 0, 1, or multiple odors. Examples shown in (A-C) are Animals 2 and 6.

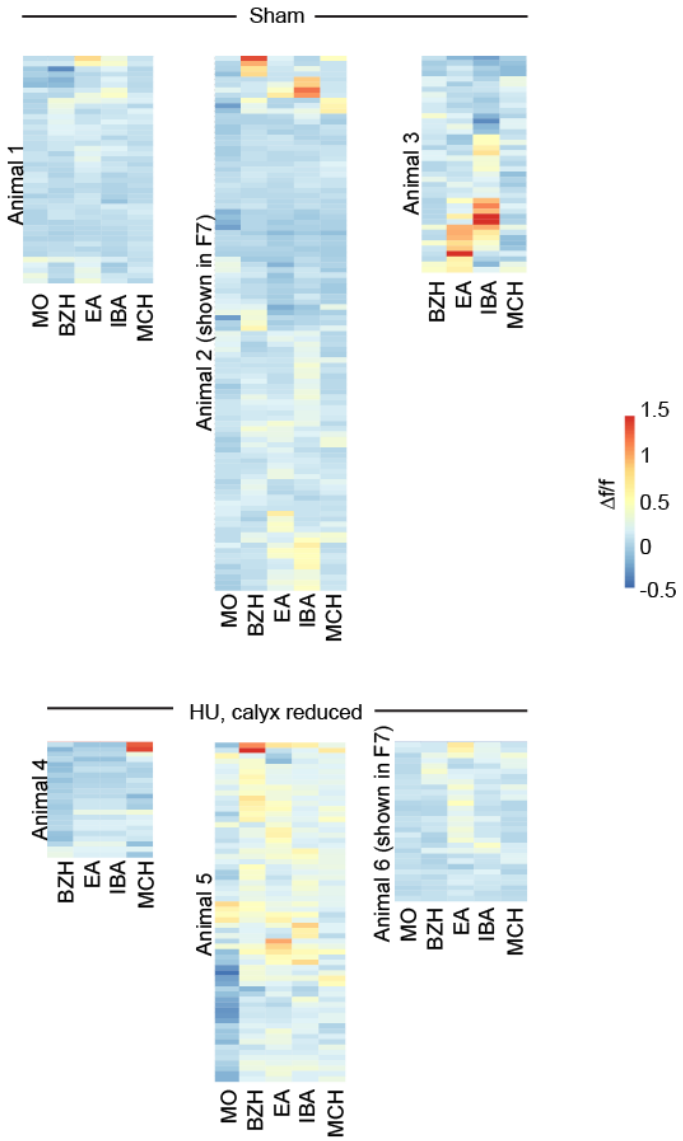

Figure S7: Supplemental data related to Figure 7. Full odor response data for each sample analyzed in Figure 7. Animals 2 and 6 are copied from Figure 7. Each row is one cell, each column is one odor. MO: Mineral oil (mechanosensory control), BZH: Benzaldehyde, EA: Ethyl Acetate, IBA: Isobutyl Acetate, MCH: Methylcyclohexanol.

598 **Discussion**

599 Cerebellum-like architectures are found repeatedly in phylogenetically distinct organisms, sug-
600 gesting that they have broad evolutionary utility. Yet the developmental production of sparse-
601 ness, a key wiring feature allowing high-dimensional sensory representations, is not understood.
602 Here, we have begun to interrogate the development of sparse connectivity in the cerebellum-
603 like associative learning center of insects, the mushroom body. By varying the ratio between
604 presynaptic olfactory PNs and postsynaptic KCs, we find that connectivity density is set by KCs:
605 KC claw number changes little across a wide range of PN::KC ratios, KC number predicts PN
606 bouton number, and PNs exhibit wide variety in bouton number to satisfy KC demands. As de-
607 scribed below, we expect that this strategy for generating connectivity density would preserve
608 sparseness in KC inputs across developmental time and upon evolutionary changes in cell rep-
609 ertoires and thus maintain the olfactory coding function of the mushroom body over a range of
610 conditions.

611

612 **Implications for development: Different projection neuron::Kenyon cell ratios across de-**
613 **velopmental stages**

614 For many animals, brain development continues while juveniles are already living freely--
615 searching for food, navigating, and learning about the environment. Developmental transitions in
616 brain structure are particularly stark in holometabolous insects, who build the brain twice. In
617 flies, neurons generated during embryonic and early larval stages wire the larval nervous sys-
618 tem. These circuits support larval behaviors, while neural stem cells continue to generate addi-
619 tional neurons that will be used to build the adult circuit. In the olfactory circuit, 21 embryoni-
620 cally-born PNs wire to early-born KCs to construct the larval mushroom body (Eichler et al.,
621 2017; Masuda-Nakagawa et al., 2005; Ramaekers et al., 2005). Connections among these pop-
622 ulations dissolve in early pupae, and are then re-wired during pupal development (Lee et al.,

623 1999; Marin et al., 2005), joined by ~100 more larvally-born PNs, and >1000 more KCs per
624 hemisphere that continue to be born until immediately before adult eclosion.
625
626 The ratio between PNs and KCs in the larval circuit is therefore starkly different from that of the
627 adult, with 21 PNs and 75 KCs forming connections in early larvae versus 150 PNs and 2000
628 KCs for the adult, a 1:3 ratio in the larva versus a 1:10 ratio in the adult (Eichler et al., 2017;
629 Zheng et al., 2018). We found that unlike cells in many other systems, including the vertebrate
630 cerebellum, PNs and KCs did not rely on each other for survival signals (Fan et al., 2001). This
631 may be due to the constantly changing ratio between these cell types across developmental
632 time. Instead, setting connectivity density cell-autonomously in KCs could allow KCs to obtain
633 the appropriate number of inputs at the different life stages of the animal, when cellular constitu-
634 ents are very different from one another. Similarly, while PN neurogenesis ceases well before
635 PNs and KCs begin to contact one another in the pupa, we estimate that ~10% of KCs are born
636 after PN:KC synapsis has already initiated (Muthukumar et al., 2014). Strict, cell-autonomous
637 dendrite structuring and flexible PN bouton production could together ensure that late-born KCs
638 obtain the inputs appropriate to support coding.
639
640 **Implications for coding: Balancing projection neuron representations across the calyx**
641 Olfactory PNs of different types are specified in a predictable temporal order, have characteristic
642 numbers of boutons, and overlap in their innervation of the calyx (Lai et al., 2008; Yu et al.,
643 2010; Zheng et al., 2018). Differences in bouton number across different PNs allow different
644 odor channels to be differentially represented in the calyx and in KC odor responses (Caron et
645 al., 2013; Honegger et al., 2011; Murthy et al., 2008). Several classes of PNs also differ in num-
646 ber between the sexes (Grabe et al., 2016). While PNs changed their individual bouton reper-
647 toires in response to changes in cell repertoires, we found that to some extent, the representa-
648 tion level of different PNs in the calyx was preserved. For example, in Figure 2F and G, we

649 show the effect of reducing KC number on bouton production by the VM6 PN and 42D01 PNs.
650 While each population of PNs reduced individual bouton number in this condition, they retained
651 their typical relative representation. The VM6 PN reduced its boutons from 10 to 5, while the
652 42D01 PNs decreased their boutons from 4 to 2. Similarly, in Figure 4, we expanded the PN
653 population by inducing ectopic PN neuroblast duplication. In these experiments, we mainly ob-
654 served amplification of the ventrolateral clone. We found that individual anterodorsal VM6 cells
655 did not scale down their boutons when the ventrolateral PN clone expanded, but only when VM6
656 itself was duplicated. Again, this could maintain the relative wild type representations of different
657 odor channels in the calyx.
658
659 **Implications for coding: Maximizing dimensionality of odor representations**
660 Qualitative aspects of sparse coding in the mushroom body appear robust to severe perturba-
661 tions to the circuit. Alternative developmental compensatory mechanisms would be much less
662 likely to preserve sparse coding. For example, we increased the ratio of PNs to KCs in two
663 ways, by increasing the number of PNs and by decreasing the number of KCs. In both cases,
664 PNs dialed down their bouton number, making 25-50% of the boutons they make in wild type.
665 This allowed the KCs to receive their typical number of inputs. If in contrast bouton number was
666 rigid and claw number flexible, in these cases KCs would have expanded their claw production
667 2-4 fold to innervate all the incoming PN boutons. Individual KCs with e.g. 20 instead of 5 claws
668 would receive input from ~40% of glomeruli, increasing the overlap in tuning across different
669 KCs and degrading the ability of the network to distinguish different stimuli from one another
670 (Litwin-Kumar et al., 2017).
671
672 In two other cases, we increased the ratio of KCs to PNs, by increasing the number of KCs and
673 by decreasing the number of PNs. Again, KCs retained their typical claw number. If instead PNs
674 had maintained a static production of boutons while KCs had adjusted their claw production,

675 KCs would receive very few inputs. While increasing the number of inputs per KC is theorized to
676 reduce dimensionality of odor responses by making different KCs more similar to one another,
677 decreasing the number of inputs per KC is theorized to reduce dimensionality by reducing the
678 number of different possible KC input combinations (Litwin-Kumar et al., 2017). That this sweet
679 spot maximizing dimensionality, ~5 inputs per cells, is programmed into KC identity testifies to
680 the evolutionary importance of maintaining connectivity density in associative brain centers that
681 rely on combinatorial coding.
682
683 **Implications for evolution: The potential for mushroom body function despite perturba-**
684 **tions**
685 The olfactory receptors are the largest insect gene family and have been subject to frequent and
686 extreme gains and losses in many clades. Similarly, brain centers devoted to learning are radi-
687 cally different across species, as exemplified by the diversity in KC repertoire across arthropods
688 (Strausfeld et al., 2009). In order to acquire a novel olfactory circuit, many different evolutionary
689 changes are required: A new receptor must evolve, an OSN type that uniquely expresses the
690 receptor needs to arise, that OSN needs to synapse onto PNs, and a new PN type and new
691 glomerulus must arise. For these events to accrue over time, each individual change must be
692 compatible with continued circuit function and olfactory behavior. While development of a dedi-
693 cated circuit that assigns an innate meaning to a newly-detectable odor would require many fur-
694 ther changes, the signal could add to fitness immediately through representation in the mush-
695 room body.
696
697 We have described two mechanisms of developmental robustness that maintain coherent
698 mushroom body wiring in the face of a broad range of phenotypic alterations. First, we observe
699 that olfactory PNs can adjust to gain and loss of PNs while maintaining the balance of odor
700 channel representations in the calyx. Plastic development of PN presynaptic sites that makes

701 room for additional players in the repertoire would allow immediate access of evolutionarily ex-
702 panded PNs to the calyx and the use of their signals for olfactory learning, thus making time for
703 the evolution of hardwired circuits for innate interpretations. Second, we show here that devel-
704 opmental programs wiring the calyx can accommodate variation in KC number from at least ¼
705 to 2-fold the endogenous complement. Again, this flexibility could support continued MB function
706 on the path to the evolution of mushroom body innovations. Future experiments will ask how KC
707 claw number is developmentally programmed, and what mechanisms operate in olfactory PNs
708 to allow them to tailor bouton production to the KC repertoire.
709
710 **Author Contributions:** JAR, NAE, and EJC performed experiments and analyzed data. EJC
711 wrote the manuscript with contributions from all authors.
712
713 **Acknowledgements**
714 We thank the Bloomington Drosophila Stock Center, Yoshi Aso, and Tzumin Lee for providing
715 fly strains; Vanessa Ruta for intellectual and material support during the early phases of this
716 project; Isaac Levine, Shiloh Boosamra, Noella Holmer, Joseph Carter, and James Harrison for
717 technical assistance; Shyama Nandakumar for help with flow cytometry experiments; Swathi
718 Yadlapalli, Yoshi Aso, Ashok Litwin-Kumar, Laura Buttitta, and members of the Cheng-Yu Lee
719 lab for experimental advice and discussion; and Cathy Collins, Monica Dus, Rich Hume,
720 Vanessa Ruta, and members of the E.J.C lab for comments on the manuscript. This work was
721 supported by the Simons Fellowship of the Helen Hay Whitney Foundation to E.J.C. E.J.C. is
722 the Rita Allen Foundation Milton Cassell Scholar and is supported by the Alfred P. Sloan Foun-
723 dation Award, and by a Neuroscience Scholar Award and start-up funds from the University of
724 Michigan.
725
726

727

728 **Methods**

729

730 *Flies:* Flies were maintained on cornmeal-molasses ("R") food (Lab Express, Ann Arbor, MI) in a

731 humidified incubator at 25C on a 12:12 light:dark cycle.

732

733 Alleles and Sources:

Allele	**Source**	**Reference**
GH146^{Gal4} (II)	BL 30026	(Stocker et al., 1997)
10XUAS-IVS-myr::tdTomato (attp40)	BL 32222	(Pfeiffer et al., 2012)
MB247-LexAVP16 (III)	Scott Waddell, University of Oxford	(Pitman et al., 2011)
LexAop-CD2-GFP (III)	BL 66544	(Lai and Lee, 2006)
GH146^{LexA} (II)	Tzumin Lee, Janelia Farms Research Campus	(Lai et al., 2008)
lexAop-mRFP-nls (II)	BL 29956	Gunter Merdes
58F02-Gal4 (attp2)	BL 39186	(Jenett et al., 2012)
UAS-GCaMP6s (attp40)	BL 42746	(Akerboom et al., 2012)
UAS-GCaMP6s (VK0005)	BL 42749	(Akerboom et al., 2012)
MB247-DsRed (II)	André Fiala	(Riemensperger et al., 2005)
71D09-Gal4 (attp2)	BL 39584	(Jenett et al., 2012)
UAS-CD8GFP (III)	BL 5130	(Lee and Luo, 1999)
42D01-Gal4 (attp2)	BL 50152	(Jenett et al., 2012)
UAS-C3PA (II)	Vanessa Ruta, Rockefeller University	(Ruta et al., 2010)

UAS-C3PA (III)	Vanessa Ruta, Rockefeller University	(Ruta et al., 2010)
60A10-LexA (attp40)	BL 52821	Pfeiffer, Rubin LexA Collection
LexAop-tdTomato.Myr (su(Hw)attp5)	BL 56142	(Chen et al., 2014)
89B01-Gal4 (attp2)	BL 40541	(Jenett et al., 2012)
13XLexAop2-IVS-Syn21-mC3PA-GFP-p10 (attp2)	Gerry Rubin, Janelia Farms Research Campus	(Pfeiffer et al., 2012)
GH146^{QF}, QUAS-mtdTomato-3xHA (II)	BL30037	(Potter et al., 2010)
UAS-mud-RNAi (attp2)	BL35044	(Perkins et al., 2015)
OK107^{Gal4} (IV)	BL 854	(Connolly et al., 1996)
P(caryP) (attp2)	BL36303	(Perkins et al., 2015)
P(caryP) (attp40)	BL36304	(Perkins et al., 2015)
MZ19^{QF} (II)	BL41573	(Hong et al., 2012)
QUAS-mtdTomato-3xHA (II)	BL 30004	(Potter et al., 2010)
41C07-LexA (attp40)	BL 54791	Pfeiffer, Rubin LexA Collection
89B01-LexA (attp40)	BL 54380	Pfeiffer, Rubin LexA Collection
71D09-LexA (attp40)	BL 54931	Pfeiffer, Rubin LexA Collection
LexAop-SPA-T2A-SPA (II)	n/a	(Clowney et al., 2015)

44F03-Gal4 (attp2)	Tzumin Lee, Janelia Farms Research Campus	(Awasaki et al., 2014)
VT033006-Gal4 (attp2)	Yoshi Aso, Janelia Farms Research Campus	(Kvon et al., 2014)
VT033008-Gal4 (attp2)	Yoshi Aso, Janelia Farms Research Campus	(Kvon et al., 2014)
UAS-DTA (UAS-Cbbeta\DT-A.I)[18] (II)	BL 25039	(Han et al., 2000)

736 Genotypes were as follows:

Figure 1	GH146^{Gal4}, 10XUAS-IVS-myr::tdTomato/CyO; MB247-lexA, lexAop-CD2-GFP/TM2
Figure 2A-E	GH146^{LexA}, lexAop-mRFP-nls/CyO; 58F02-Gal4, UAS-GCaMP6s/TM2
Figure 2F	MB247-DsRed/CyO; 71D09-Gal4, UAS-CD8GFP/"
Figure 2G	MB247-DsRed/CyO; 42D01-Gal4, UAS-C3PA/"
Figure 2H	60A10-LexA, LexAop-tdTomato.Myr/CyO; 58F02-Gal4, UAS-C3PA/"
Figure 2I	GH146^{Gal4}, 10XUAS-IVS-myr::tdTomato /CyO; MB247-lexA, 13XLexAop2-IVS-Syn21-mC3PA-GFP-p10/"
	60A10-LexA, LexAop-tdTomato.Myr /CyO; 58F02-Gal4, UAS-C3PA/"
	60A10-LexA, LexAop-tdTomato.Myr /CyO; 89B01-Gal4, UAS-C3PA/"
Figure S2A, B	GH146^{LexA}, lexAop-mRFP-nls /CyO; 58F02-Gal4, UAS-GCaMP6s/TM2
Figure S2C, D	GH146^{Gal4}, 10XUAS-IVS-myr::tdTomato /CyO; MB247-lexA, 13XLexAop2-IVS-Syn21-mC3PA-GFP-p10/"
Figure S2E	60A10-LexA, LexAop-tdTomato.Myr /CyO; 58F02-Gal4, UAS-C3PA/"
Figure S2F	60A10-LexA, LexAop-tdTomato.Myr /CyO; 89B01-Gal4, UAS-C3PA/"
Figure 3A, B	GH146^{QF}, QUAS-mtdTomato-3xHA /+; UAS-CD8GFP/UAS-mud-RNAi; OK107^{Gal4}/+
	GH146^{QF}, QUAS-mtdTomato-3xHA /+; UAS-CD8GFP/ P(caryP)attp2; OK107^{Gal4}/+
Figure 3C-E	MZ19^{QF}, QUAS-mtdTomato-3xHA /Bl; UAS-mud-RNAi/TM2 or TM6B; OK107^{Gal4}/+
	MZ19^{QF}, QUAS-mtdTomato-3xHA /Bl; P(caryP)attp2/TM2 or TM6B; OK107/+
Figure3F, G	UAS-C3PA/+; UAS-C3PA/ UAS-mud-RNAi; OK107^{Gal4}/+
	UAS-C3PA/+; UAS-C3PA/ P(caryP)attp2; OK107^{Gal4}/+
	UAS-C3PA/41C07-LexA, LexAop-tdTomato.Myr; UAS-C3PA/ UAS-mud-RNAi; OK107^{Gal4}/+
	UAS-C3PA/41C07-LexA, LexAop-tdTomato.Myr; UAS-C3PA/ P(caryP)attp2; OK107 ^{Gal4}/+
	UAS-C3PA/89B01-LexA, LexAop-tdTomato.Myr; UAS-C3PA/ UAS-mud-RNAi; OK107 ^{Gal4}/+
	UAS-C3PA/89B01-LexA, LexAop-tdTomato.Myr; UAS-C3PA/ P(caryP)attp2; OK107 ^{Gal4}/+
Figure S3A	71D09-LexA, LexAop-tdTomato.Myr /Bl; UAS-mud-RNAi/TM2; OK107 ^{Gal4}/+
	71D09-LexA, LexAop-tdTomato.Myr /Bl; P(caryP)attp2/TM2; OK107 ^{Gal4}/+
Figure S3B	41C07-LexA, LexAop-tdTomato.Myr /UAS-C3PA; UAS-mud-RNAi 35044/UAS-C3PA; OK107 ^{Gal4}/+
	41C07-LexA, LexAop-tdTomato.Myr /UAS-C3PA; P(caryP)attp2/UAS-C3PA; OK107 ^{Gal4}/+
Figure 4A-F	GH146^{LexA}, LexAop-SPA-T2A-SPA /+; 44F03-Gal4/ UAS-mud-RNAi
	GH146^{LexA}, LexAop-SPA-T2A-SPA /+; 44F03-Gal4/ P(caryP)attp2
Figure 4G, H	GH146^{LexA}, LexAop-SPA-T2A-SPA /MZ19^{QF}, QUAS-mtdTomato-3xHA; 44F03-Gal4/ UAS-mud-RNAi

	GH146^{LexA}, LexAop-SPA-T2A-SPA /MZ19^{QF}, QUAS-mtdTomato-3xHA; 44F03-Gal4/ P(caryP)attp2
	MZ19^{QF}, QUAS-mtdTomato-3xHA /+; 44F03-Gal4/ UAS-mud-RNAi
	MZ19^{QF}, QUAS-mtdTomato-3xHA /+; 44F03-Gal4/ P(caryP)attp2
Figure S4A	GH146^{LexA}, LexAop-SPA-T2A-SPA /+; 44F03-Gal4/ UAS-mud-RNAi
	GH146^{LexA}, LexAop-SPA-T2A-SPA /+; 44F03-Gal4/ P(caryP)attp2
Figure S4B, C	71D09-LexA, LexAop-tdTomato.Myr /+; 44F03-Gal4/ UAS-mud-RNAi
	71D09-LexA, LexAop-tdTomato.Myr /+; 44F03-Gal4 P(caryP)attp2
Figure 5A	CyO/+; VT033006-Gal4/UAS-CD8GFP
	CyO/+; VT033008-Gal4/UAS-CD8GFP
Figure5B, C	GH146^{LexA}, lexAop-mRFP-nls /UAS-DTA; VT033008-Gal4, UAS-CD8GFP/+
	GH146^{LexA}, lexAop-mRFP-nls / P(caryP)attp40; VT033008-Gal4, UAS-CD8GFP/+
Figure5D, E	UAS-DTA/+; VT033008-Gal4/TM6B
	UAS-DTA/+; P(caryP)attp2/TM6B
Figure5F, G	GH146^{LexA}, lexAop-mRFP-nls / UAS-DTA; VT033006-Gal4, UAS-CD8GFP/+
	GH146^{LexA}, lexAop-mRFP-nls / P(caryP)attp40; VT033006-Gal4, UAS-CD8GFP/+
Figure5H-J	MB247-DsRed/ UAS-DTA; VT033006-Gal4, UAS-CD8GFP/+
	MB247-DsRed/+; VT033006-Gal4, UAS-CD8GFP/+
Figure S5	MB247-DsRed/ UAS-DTA; VT033006-Gal4, UAS-CD8GFP/+
	MB247-DsRed/+; VT033006-Gal4, UAS-CD8GFP/+
Figure6	GH146^{LexA}, LexAop-SPA-T2A-SPA / UAS-DTA; VT033006-Gal4/+
	GH146^{LexA}, LexAop-SPA-T2A-SPA / P(caryP)attp40; VT033006-Gal4/+
Figure 7, S7	UAS-GCaMP6s/UAS-GCaMP6s; UAS-GCaMP6s/UAS-GCaMP6s; OK107^{Gal4}/ OK107^{Gal4} or +

HU ablation: Protocol was adapted from Sweeney et al (Sweeney et al., 2012). Briefly, we set up large populations of flies in cages two days prior to ablation and placed a 35 or 60mm grape juice agar plate (Lab Express, Ann Arbor, MI) in the cage with a dollop of goopy yeast. One day prior to the ablation, we replaced the grape juice/yeast plate with a new grape juice/yeast plate. On the morning of the ablation, we removed the plate from the cage one hour after lights-on and discarded the yeast puck and any hatched larvae on the agar. We then monitored the plate for up to four hours, until many larvae had hatched. Larvae were washed off the plate using a sucrose solution, and eggs were discarded. Larvae were then strained in coffee filters, and

746 submerged in hydroxyurea in a yeast:AHL mixture, or sham mixture without HU. Ablation condi-
747 tions were as follows:
748 Figure 1: 10mg/mL or 5mg/mL, 4 hours
749 Figure 2A-G: 10mg/mL, 1 hour
750 Figure 2H, I: 10mg/mL, 1 hour; 3 or 5 mg/mL, 4 hours
751 Figure 7: 10mg/mL, 1 hour
752
753 Larvae were then strained through coffee filters again, rinsed, and placed in a vial or bottle of R
754 food until eclosion. We opened a new container of hydroxyurea each month as it degrades in
755 contact with moisture and we found its potency gradually declined. We typically analyzed 5-10
756 animals (10-20 hemispheres) of each condition per batch, except in *in vivo* imaging experi-
757 ments, where we analyzed 1-3 animals per condition per batch.
758
759 Applying HU for four hours produced a somewhat U-shaped distribution, with many samples un-
760 affected and many with all four KC neuroblasts lost. Shifting from 3, to 5, to 10 mg over this long
761 time scale shifted how many brains were completely ablated versus unaffected, but did little to
762 increase the proportion of brains with intermediate phenotypes. Applying the stronger concen-
763 tration, 10mg, for a shorter time produced more sporadic effects, with more brains showing 1, 2,
764 or 3 KC neuroblasts remaining. lNB/BAlc was more affected by HU concentration than time of
765 application, with stronger effects seen applying 10mg/mL for one hour than applying 3 or
766 5mg/mL for four hours. Overall, combining these different protocols allowed us to observe a
767 broad range of mushroom body states.
768
769 *Immunostainings:* Brains were dissected for up to 20 minutes in external saline (108 mM NaCl,
770 5 mM KCl, 2 mM CaCl2, 8.2 mM MgCl2, 4 mM NaHCO3, 1 mM NaH2PO4, 5 mM trehalose, 10
771 mM sucrose, 5 mM HEPES pH7.5, osmolarity adjusted to 265 mOsm), before being transferred

772 to 1% paraformaldehyde in PBS, on ice. All steps were performed in cell strainer baskets (caps
773 of FACS tubes) in 24 well plates, with the brains in the baskets lifted from well to well to change
774 solutions. Brains were fixed overnight at 4C in 1% PFA in PBS. On day 2, brains were washed
775 3x10' in PBS supplemented with 0.1% triton-x-100 on a shaker at room temperature, blocked 1
776 hour in PBS, 0.1% triton, 4% Normal Goat Serum, and then incubated for at least two over-
777 nights in primary antibody solution, diluted in PBS, 0.1% triton, 4% Normal Goat Serum. Primary
778 antibody was washed 3x10' in PBS supplemented with 0.1% triton-x-100 on a shaker at room
779 temperature, then brains were incubated in secondary antibodies for at least two overnights, di-
780 luted in PBS, 0.1% triton, 4% Normal Goat Serum. When used, Alexa 568-conjugated phalloidin
781 (1:80) and/or DAPI (1 microgram/mL) were included in secondary antibody mixes. Primary anti-
782 bodies used were mouse anti-ChaT 9E10 (DSHB, 1:200), Rabbit anti-dsRed (Clontech, 1:1000),
783 Sheep anti-GFP (Bio-Rad, 4745-1051, 1:1000), Chicken anti-GFP (1:5000, gift from Dawen
784 Cai). Secondary antibodies were Alexa 488, 568, and 647 conjugates (1:500, Invitrogen).
785
786 Brains were mounted in 1x PBS, 90% glycerol supplemented with propyl gallate in binder rein-
787 forcement stickers sandwiched between two coverslips. Samples were stored at 4C in the dark
788 prior to imaging. The coverslip sandwiches were taped to slides, allowing us to perform confocal
789 imaging on one side of the brain and then flip over the sandwich to allow a clear view of the
790 other side of the brain. This allowed us to score features on the anterior and posterior sides of
791 each sample. Scanning confocal stacks were collected on a Zeiss 710 or Leica SP8 at 40x
792 magnification, with ~150nm x 150nm pixels and 1 micrometer spacing in Z.
793
794 Genotypes or conditions being compared with one another were always prepared for staining
795 together and imaged interspersed with one another to equalize batch effects.
796

797 *Image analysis:* In general, we analyzed mixed-sex populations, where sex ratios were carefully
798 balanced across experimental conditions. Because MZ19 labels the sexually dimorphic DA1
799 PNs, in MZ19 experiments we analyzed the two sexes independently in pilot experiments. As
800 we observed no correlation with sex (not shown), in subsequent MZ19 experiments we used
801 mixed sexes.
802
803 Researchers performing quantification could not generally be blinded to experimental condition
804 due to the overt changes in neuron numbers and brain structures induced by our manipulations.
805 However, analysis was performed blind to the goals of the experiment when possible, and quan-
806 titation of features on the anterior and posterior sides of the brain were recorded independent of
807 one another and merged after all quantifications were completed. Moreover, many of our anal-
808 yses make use of variation within an experimental condition or genotype, providing an additional
809 bulwark against observational bias.
810
811 To measure neuropil structures such as the mushroom body calyx, lateral horn, or antennal
812 lobe, we used markers such as ChAT and phalloidin to visualize the structure, identified its larg-
813 est extent in Z, outlined it in FIJI, and then calculated the cross-sectional area using the "Meas-
814 ure" command.
815
816 To count aggregate boutons, we used ChAT signal with reference to phalloidin (which stains ac-
817 tin-rich structures, including KC dendrites), except in Figure 1, where we counted GH146-posi-
818 tive boutons. We counted as separate structures ChAT signals that were compact and ap-
819 peared discontinuous with one another and that were ~1-2 micrometers in diameter. When phal-
820 loidin signal or KC fluorescence was available, two boutons would be counted separately if
821 ChAT signals were separated by phalloidin signal or KC signal. We began counting at the first
822 slice in the stack where boutons were visible, and counted every other slice. To count boutons

823 of small groups of PNs, we drove fluorescent reporters under control of 42D01, 71D09, or MZ19
824 and counted coherent and compact fluorescent signals, with reference to ChAT signals and to
825 phalloidin, when available. Our bouton counts (~1000/calyx) correspond with other quantifica-
826 tions performed by light microscopy, but differ from the <600 boutons/calyx recently identified by
827 EM (Leiss et al., 2009; Zheng et al., 2018).
828 To count cell populations, we used genetically-encoded fluorescence as indicated. We counted
829 labeled somata in every third slice in the stack, with reference to DAPI to distinguish individual
830 cells from one another.
831
832 To count KC claws, we scanned image stacks for cup-shaped terminal structures of the appro-
833 priate size (1-2μm in diameter). In Figures 2I, 3G, and 6F, we sometimes labeled small groups
834 of KCs. We scored independently any single KC or small group of KCs that could be visually
835 separated from one another (like the 3 cells shown in Figure 6C). For Figure 2I, we did not
836 score any cells which we could not separate from one another because we did not want to mix
837 counts for KCs of different types. For Figure 3G, where we did not attempt to separate KCs of
838 different types, and Figure 6F, where our dye labeling strategy was specific to αβ KCs, we pre-
839 sent an average claw/KC data point for small groups of 2-4 cells whose dendritic structures
840 were interwoven. Finally, in Figure 3G, we found that in calyces with expanded KC populations,
841 KC axons sometimes could not enter the pedunculus and instead wandered around at the base
842 of the calyx. As CNS neurons in *D. mel* are unipolar, these wandering axons could be difficult to
843 distinguish from dendritic claws. To determine whether these wandering axons should be
844 counted as claws, we stained a subset of photoactivated brains with anti-ChAT (not shown), to
845 determine which labeled KC neurites were in the bouton region of the calyx, and should thus be
846 scored for claws, and which were “lost” axons. Though photoactivated GFP signals were only
847 poorly preserved following staining, relating ChAT-stained images to images of the same brain

848 by two photon allowed us to learn to identify the bouton region of the calyx in subsequent exper-
849 iments due to its “swiss cheese” appearance, where the presence of PN boutons produces
850 holes in KC fluorescence.
851
852 To determine KC and PN neuroblast state--PN lNB/BAlc: In Figure 1 and Figure 2A-C, we in-
853 cluded GH146 driving a fluorescent report in our animals and scored the presence or absence
854 of a group of somata lateral to the antennal lobe on the anterior side of the brain for each ana-
855 lyzed hemisphere. For Figure 2 F-G, including such a marker was incompatible with the geno-
856 types used to label small PN groups and we were thus blind to, and do not report, lNB/BAlc sta-
857 tus. Based on the typical sample distributions we observed (Figure S2), we assume that some
858 brains of each status were among the samples analyzed in Figure 2 F-G. For Figure 2H-I, we
859 scored lNB/BAlc status using either 60A10 LexA or GH146 Gal4 to label PNs lateral to the an-
860 tennal lobe. For clarity, we do not report lNB/BAlc status in Figures 2H, but include this infor-
861 mation in Figure S2. KC neuroblasts: In Figures 2A-C, we used 58F02 to fluorescently label
862 late-born KCs and counted clumps of labeled somata surrounding the calyx as well as groups of
863 labeled neurites leaving the calyx and entering the pedunculus. These estimates usually
864 matched; in the few cases where they did not, we used the number of axon clumps, as somata
865 are closer to the surface of the brain and more susceptible to mechanical disruption during dis-
866 section. In Figure 2F, G, because we found a linear relationships between KC number and calyx
867 size, and between KC neuroblast number and calyx size, we used calyx size to infer KC neuro-
868 blast state. To do so, we calculated the average calyx area for HU treated samples that lacked
869 vertical lobes as the “0 KC neuroblast” condition, and sham-treated calyces as the “4 KC neuro-
870 blast” condition. We then divided this range evenly into bins for 1, 2, and 3 neuroblasts as
871 shown in Figure S2G.
872

873 For Figures 2H, I we combined data from two different types of experiments. In some experi-
874 ments, we expressed PA-GFP in all KCs using MB247. We traced the axons of labeled KCs into
875 the lobes to assign KC type. For these samples, we inferred KC neuroblast state by measuring
876 calyx size, as above. While we do not report data points for αβ or γ KCs in 0-KC-neuroblast
877 brains, since no αβ or γ KCs are born in this case, we used signal derived from remaining γd
878 KCs to measure calyx area in these samples. In a second group of experiments, we used
879 58F02-Gal4 to express PA-GFP exclusively in αβ core KCs, or 89B01 Gal4 to express PA-GFP
880 only in γ KCs. In 58F02-labeled brains, we counted KC neuroblasts as above. In 89B01 brains,
881 we counted how many "holes" there were in the labeled cloud of KC somata to define KC neuro-
882 blast number (89B01 labels early- but not late-born KCs, the inverse of 58F02). Because the
883 number of informative hemispheres using each of these approaches was low (i.e. most HU
884 treated brains had 0 or 4 KC neuroblasts left), to make the graphs in Figure 2I, we combined the
885 results of these two approaches. Points from each approach are disaggregated in Figure S2
886 and no trends toward increased KC claw number in brains with few KCs were observed using
887 either of the individual approaches.
888
889 *GFP photoactivation and Texas red dextran dye labeling* were performed as previously de-
890 scribed (Clowney et al., 2015; Ruta et al., 2010), using a Bruker Investigator microscope and
891 Spectra-Physics MaiTai laser with DeepSee module. Dye filling electrodes were pulled using a
892 Brown/Flaming puller (Sutter Instruments) and were guided to the mushroom body alpha lobes
893 using visible light illumination and/or two photon autofluorescence.
894
895 *Identification of driver lines for relevant cell populations*: To identify Gal4 and/or LexA lines la-
896 beling PN populations, we screened the Janelia FlyLight collection online database and then
897 crossed lines with potential to fluorescent reporters. While 42D01 (~10PNs) and 60A10 (60

898 PNs) were the most useful PN lines for us here, we also identified other lines, 33C10 and
899 37H08, that each label small groups of PNs and may be of use to others. To identify Gal4 lines
900 labeling individual KC types, we screened expression of "regular" FlyLight Gal4 constructs made
901 using the same regulatory fragments incorporated in KC-type-specific split Gal4s (Aso et al.,
902 2014). We found 58F02 useful for labeling α/β core KCs, 89B01 for γ KCs (labels both γmain
903 and γd), and 41C07 for α'/β' KCs. At the time we did this screen, only 89B01 and 41C07 were
904 available as LexA lines; 89B01 LexA did not recapitulate 89B01 Gal4 expression.
905
906 *Flow Cytometry*: Brains were dissected in Schneider's medium (Sigma S0146) supplemented
907 with 1% BSA and placed on ice. After all dissections were completed, collagenase (Sigma
908 C0130) was added to a final concentration of 2mg/mL and samples were incubated at 37C for
909 20 minutes. Samples were dissociated by trituration and spun down at 300g, 4C, for 5 minutes.
910 Collagenase solution was removed and replaced with PBS+0.1% BSA supplemented with
911 1:1000 DyeCycle Violet. Cells were incubated with dye for 30 minutes on ice and passed
912 through a cell strainer cap, before being subjected to flow cytometry on an Attune Flow Cytome-
913 ter. Forward scatter and side scatter measurements were used to gate single cells, and DyeCy-
914 cle Violet signal was used to gate cell bodies from membrane debris.
915
916 *In vivo functional imaging*: We prepared 2-7 day old adult female flies subjected to HU or sham
917 treatment just after larval hatching for *in vivo* two photon calcium on a Bruker Investigator es-
918 sentially as described previously (Ruta et al., 2010), with the fly tilted to allow optical access to
919 KC somata, at the dorsal posterior surface of the brain. Imaging was performed in external sa-
920 line. For odor delivery, half of a 1200mL/min airstream, or 600mL/min, was directed toward the
921 antennae through a Pasteur pipette mounted on a micromanipulator. At a trigger, 25% of the to-
922 tal air stream was re-directed from a 10mL glass vial containing mineral oil to a vial containing

923 odorants diluted 1:10 in mineral oil. Final odor dilution was therefore 1:40. Filter paper “wicks”
924 were inserted into each vial to allow odor to saturate the vial headspace. Odors were delivered
925 for two seconds, with 30 seconds in between stimulations. We used a simplified olfactometer
926 capable of delivering five different odorants in which overall airflow was metered by analogue
927 flowmeters (Brooks Instruments) and valve switching controlled by an Arduino. Odor delivery
928 was initially optimized using a mini-PID (Aurora Biosciences). Images were collected at 1.5-3
929 Hertz. We imaged eight sham-treated and 11 HU treated animals. Complete data was collected
930 for 12 and 19 hemispheres, respectively, due to lack of odor responses or clear physical dam-
931 age in a subset of samples. Importantly, the proportion of samples that were not odor respon-
932 sive was not higher among ablated animals than among controls, consistent with the non-re-
933 sponsive samples being due to preparation failure. For each HU treatment batch and sham con-
934 trol, we imaged animals from both conditions.
935
936 *Analysis of KC somatic odor responses*: Time series for each sample were motion-corrected us-
937 ing Suite2p (Pachitariu et al., 2017), and an ROI for each cell manually defined in FIJI. Sufficient
938 stability to identify the same cell across a stimulation series was difficult to achieve given that
939 KC somata are densely packed and only 2μm in diameter, and that animals were robustly active
940 during imaging; samples in which ROIs were not spatially stable over different stimulations were
941 not analyzed further. Among HU treated samples, we could clearly delineate between samples
942 lacking all olfactory KCs (lacking vertical lobes), samples with strong reduction in KCs, and sam-
943 ples with calyces similar to sham controls. Though we recovered brains for immunostaining and
944 cell counting after functional imaging (as shown in example in Figure 7), damage to the brain
945 during post-imaging surgery prevented us from making finer distinctions among calyx types. We
946 therefore analyzed three brains with intermediate KC losses as one treatment group. The three
947 sham-treated animals analyzed were those that were sufficiently still to allow analysis.
948

949 For each ROI in each of six samples, we measured $\Delta f/f$ (i.e. $(f-f_0)/f_0$), comparing stimulus frames
950 with pre-stimulus frames. To define "responsive" cells, we chose to use the same cutoff, $\Delta f/f$
951 >0.2 (20% increase in fluorescence over baseline) across samples. This was in order to avoid
952 obscuring overall differences in responsiveness across ablated and sham-treated calyces. Us-
953 ing this method, the proportion of cells responding to each odor were generally greater, in both
954 control and treatment conditions, than what has been described previously (Honegger et al.,
955 2011). Differences are thus likely due to differences in GCaMP variant (GCaMP6s versus
956 GCaMP3), odor concentration (1:40 versus 1:100 dilution), and thresholding method ($\Delta f/f$ cutoff
957 common to all samples versus determined by standard deviation from baseline within each
958 sample). The overall level of variation we observe across control samples is similar to what has
959 been reported previously (Honegger et al., 2011). For visualization, we used the Pretty Heatmap
960 package in R to cluster cells with similar odor responses and display them.
961

962 **References**

963 Akerboom J, Chen T-W, Wardill TJ, Tian L, Marvin JS, Mutlu S, Calderón NC, Esposti F, Bor-
964 ghuis BG, Sun XR, Gordus A, Orger MB, Portugues R, Engert F, Macklin JJ, Filosa A,
965 Aggarwal A, Kerr RA, Takagi R, Kracun S, Shigetomi E, Khakh BS, Baier H, Lagnado L,
966 Wang SS-H, Bargmann CI, Kimmel BE, Jayaraman V, Svoboda K, Kim DS, Schreiter
967 ER, Looger LL. 2012. Optimization of a GCaMP calcium indicator for neural activity im-
968 aging. *J Neurosci Off J Soc Neurosci* **32**:13819–13840. doi:10.1523/JNEUROSCI.2601-
969 12.2012
970 Albus JS. 1971. A theory of cerebellar function. *Math Biosci* **10**:25–61. doi:10.1016/0025-
971 5564(71)90051-4
972 Aso Y, Hattori D, Yu Y, Johnston RM, Iyer NA, Ngo T-TB, Dionne H, Abbott LF, Axel R, Tan-
973 imoto H, Rubin GM. 2014. The neuronal architecture of the mushroom body provides a
974 logic for associative learning. *eLife* **3**:e04577. doi:10.7554/eLife.04577
975 Awasaki T, Kao C-F, Lee Y-J, Yang C-P, Huang Y, Pfeiffer BD, Luan H, Jing X, Huang Y-F, He
976 Y, Schroeder MD, Kuzin A, Brody T, Zugates CT, Odenwald WF, Lee T. 2014. Making
977 *Drosophila* lineage–restricted drivers via patterned recombination in neuroblasts. *Nat*
978 *Neurosci* **17**:631. doi:10.1038/nn.3654
979 Bell CC, Han V, Sawtell NB. 2008. Cerebellum-like structures and their implications for cerebel-
980 lar function. *Annu Rev Neurosci* **31**:1–24. doi:10.1146/annurev.neuro.30.051606.094225
981 Berdnik D, Chihara T, Couto A, Luo L. 2006. Wiring Stability of the Adult Drosophila Olfactory
982 Circuit after Lesion. *J Neurosci* **26**:3367–3376. doi:10.1523/JNEUROSCI.4941-05.2006
983 Caron SJC, Ruta V, Abbott LF, Axel R. 2013. Random convergence of olfactory inputs in the
984 Drosophila mushroom body. *Nature* **497**:113–117. doi:10.1038/nature12063

985 Cayco-Gajic NA, Clopath C, Silver RA. 2017. Sparse synaptic connectivity is required for decor-
986 relation and pattern separation in feedforward networks. *Nat Commun* **8**:1116.
987 doi:10.1038/s41467-017-01109-y
988 Chabrol FP, Arenz A, Wiechert MT, Margrie TW, DiGregorio DA. 2015. Synaptic diversity ena-
989 bles temporal coding of coincident multisensory inputs in single neurons. *Nat Neurosci*
990 **18**:718–727. doi:10.1038/nn.3974
991 Chen Y, Akin O, Nern A, Tsui CYK, Pecot MY, Zipursky SL. 2014. Cell-type-Specific Labeling of
992 Synapses In Vivo through Synaptic Tagging with Recombination. *Neuron* **81**:280–293.
993 doi:10.1016/j.neuron.2013.12.021
994 Chin SG, Maguire SE, Huoviala P, Jefferis GSXE, Potter CJ. 2018. Olfactory Neurons and Brain
995 Centers Directing Oviposition Decisions in Drosophila. *Cell Rep* **24**:1667–1678.
996 doi:10.1016/j.celrep.2018.07.018
997 Clowney EJ, Iguchi S, Bussell JJ, Scheer E, Ruta V. 2015. Multimodal Chemosensory Circuits
998 Controlling Male Courtship in Drosophila. *Neuron* **87**:1036–1049. doi:10.1016/j.neu-
999 ron.2015.07.025
1000 Cohn R, Morantte I, Ruta V. 2015. Coordinated and Compartmentalized Neuromodulation
1001 Shapes Sensory Processing in Drosophila. *Cell* **163**:1742–1755.
1002 doi:10.1016/j.cell.2015.11.019
1003 Connolly JB, Roberts IJH, Armstrong JD, Kaiser K, Forte M, Tully T, O'Kane CJ. 1996. Associa-
1004 tive Learning Disrupted by Impaired Gs Signaling in Drosophila Mushroom Bodies. *Sci-*
1005 *ence* **274**:2104–2107. doi:10.1126/science.274.5295.2104
1006 Corty MM, Tam J, Grueber WB. 2016. Dendritic diversification through transcription factor-medi-
1007 ated suppression of alternative morphologies. *Development* **143**:1351–1362.
1008 doi:10.1242/dev.130906
1009 Das A, Gupta T, Davla S, Prieto-Godino LL, Diegelmann S, Reddy OV, Raghavan KV, Reichert
1010 H, Lovick J, Hartenstein V. 2013. Neuroblast lineage-specific origin of the neurons of the
1011 Drosophila larval olfactory system. *Dev Biol* **373**:322–337. doi:10.1016/j.yd-
1012 bio.2012.11.003
1013 de Belle JS, Heisenberg M. 1994. Associative odor learning in Drosophila abolished by chemi-
1014 cal ablation of mushroom bodies. *Science* **263**:692–695.
1015 Eichler K, Li F, Litwin-Kumar A, Park Y, Andrade I, Schneider-Mizell CM, Saumweber T, Huser
1016 A, Eschbach C, Gerber B, Fetter RD, Truman JW, Priebe CE, Abbott LF, Thum AS,
1017 Zlatic M, Cardona A. 2017. The complete connectome of a learning and memory centre
1018 in an insect brain. *Nature* **548**:175–182. doi:10.1038/nature23455
1019 Fan H, Favero M, Vogel MW. 2001. Elimination of bax expression in mice increases cerebellar
1020 purkinje cell numbers but not the number of granule cells. *J Comp Neurol* **436**:82–91.
1021 doi:10.1002/cne.1055
1022 Farris SM. 2011. Are mushroom bodies cerebellum-like structures? *Arthropod Struct Dev*
1023 **40**:368–379. doi:10.1016/j.asd.2011.02.004
1024 Fişek M, Wilson RI. 2014. Stereotyped connectivity and computations in higher-order olfactory
1025 neurons. *Nat Neurosci* **17**:280–288. doi:10.1038/nn.3613
1026 Gibbins IL, Teo EH, Jobling P, Morris JL. 2003. Synaptic density, convergence, and dendritic
1027 complexity of prevertebral sympathetic neurons. *J Comp Neurol* **455**:285–298.
1028 doi:10.1002/cne.10404
1029 Grabe V, Baschwitz A, Dweck HKM, Lavista-Llanos S, Hansson BS, Sachse S. 2016. Elucidat-
1030 ing the Neuronal Architecture of Olfactory Glomeruli in the Drosophila Antennal Lobe.
1031 *Cell Rep* **16**:3401–3413. doi:10.1016/j.celrep.2016.08.063
1032 Gruntman E, Turner GC. 2013. Integration of the olfactory code across dendritic claws of single
1033 mushroom body neurons. *Nat Neurosci* **16**:1821–1829. doi:10.1038/nn.3547

1034 Guan Z, Prado A, Melzig J, Heisenberg M, Nash HA, Raabe T. 2000. Mushroom body defect, a
1035 gene involved in the control of neuroblast proliferation in Drosophila, encodes a coiled–
1036 coil protein. *Proc Natl Acad Sci* **97**:8122–8127. doi:10.1073/pnas.97.14.8122
1037 Han DD, Stein D, Stevens LM. 2000. Investigating the function of follicular subpopulations dur-
1038 ing Drosophila oogenesis through hormone-dependent enhancer-targeted cell ablation.
1039 *Dev Camb Engl* **127**:573–583.
1040 Handler A, Graham TGW, Cohn R, Morantte I, Siliciano AF, Zeng J, Li Y, Ruta V. 2019. Distinct
1041 Dopamine Receptor Pathways Underlie the Temporal Sensitivity of Associative Learn-
1042 ing. *Cell* **178**:60-75.e19. doi:10.1016/j.cell.2019.05.040
1043 Hige T. 2018. What can tiny mushrooms in fruit flies tell us about learning and memory? *Neuro-*
1044 *sci Res* **129**:8–16. doi:10.1016/j.neures.2017.05.002
1045 Hige T, Aso Y, Rubin GM, Turner GC. 2015. Plasticity-driven individualization of olfactory cod-
1046 ing in mushroom body output neurons. *Nature* **526**:258–262. doi:10.1038/nature15396
1047 Honegger KS, Campbell RAA, Turner GC. 2011. Cellular-resolution population imaging reveals
1048 robust sparse coding in the Drosophila mushroom body. *J Neurosci Off J Soc Neurosci*
1049 **31**:11772–11785. doi:10.1523/JNEUROSCI.1099-11.2011
1050 Hong W, Mosca TJ, Luo L. 2012. Teneurins instruct synaptic partner matching in an olfactory
1051 map. *Nature* **484**:201–207. doi:10.1038/nature10926
1052 Huang C-C, Sugino K, Shima Y, Guo C, Bai S, Mensh BD, Nelson SB, Hantman AW. 2013.
1053 Convergence of pontine and proprioceptive streams onto multimodal cerebellar granule
1054 cells. *eLife* **2**:e00400. doi:10.7554/eLife.00400
1055 Hume RI, Purves D. 1983. Apportionment of the terminals from single preganglionic axons to
1056 target neurones in the rabbit ciliary ganglion. *J Physiol* **338**:259–275. doi:10.1113/jphys-
1057 iol.1983.sp014672
1058 Hume RI, Purves D. 1981. Geometry of neonatal neurones and the regulation of synapse elimi-
1059 nation. *Nature* **293**:469–471.
1060 Ishikawa T, Shimuta M, Häusser M. 2015. Multimodal sensory integration in single cerebellar
1061 granule cells in vivo. *eLife* **4**:e12916. doi:10.7554/eLife.12916
1062 Ito K, Awano W, Suzuki K, Hiromi Y, Yamamoto D. 1997. The Drosophila mushroom body is a
1063 quadruple structure of clonal units each of which contains a virtually identical set of neu-
1064 rones and glial cells. *Development* **124**:761–771.
1065 Ito K, Hotta Y. 1992. Proliferation pattern of postembryonic neuroblasts in the brain of Drosoph-
1066 ila melanogaster. *Dev Biol* **149**:134–148. doi:10.1016/0012-1606(92)90270-Q
1067 Jan Y-N, Jan LY. 2010. Branching out: mechanisms of dendritic arborization. *Nat Rev Neurosci*
1068 **11**:316–328. doi:10.1038/nrn2836
1069 Jefferis GSXE, Potter CJ, Chan AM, Marin EC, Rohlfing T, Maurer CR, Luo L. 2007. Compre-
1070 hensive maps of Drosophila higher olfactory centers: spatially segregated fruit and pher-
1071 omone representation. *Cell* **128**:1187–1203. doi:10.1016/j.cell.2007.01.040
1072 Jefferis GSXE, Vyas RM, Berdnik D, Ramaekers A, Stocker RF, Tanaka NK, Ito K, Luo L. 2004.
1073 Developmental origin of wiring specificity in the olfactory system of Drosophila. *Dev*
1074 *Camb Engl* **131**:117–130. doi:10.1242/dev.00896
1075 Jenett A, Rubin GM, Ngo T-TB, Shepherd D, Murphy C, Dionne H, Pfeiffer BD, Cavallaro A, Hall
1076 D, Jeter J, Iyer N, Fetter D, Hausenfluck JH, Peng H, Trautman ET, Svirskas RR, Myers
1077 EW, Iwinski ZR, Aso Y, DePasquale GM, Enos A, Hulamm P, Lam SCB, Li H-H, Laverty
1078 TR, Long F, Qu L, Murphy SD, Rokicki K, Safford T, Shaw K, Simpson JH, Sowell A,
1079 Tae S, Yu Y, Zugates CT. 2012. A GAL4-Driver Line Resource for Drosophila Neurobiol-
1080 ogy. *Cell Rep* **2**:991–1001. doi:10.1016/j.celrep.2012.09.011
1081 Keene AC, Waddell S. 2007. Drosophila olfactory memory: single genes to complex neural cir-
1082 cuits. *Nat Rev Neurosci* **8**:341–354. doi:10.1038/nrn2098
1083 Kennedy A. 2015. Representation and learning in cerebellum-like structures. Columbia Univer-
1084 sity. doi:10.7916/D8DV1HM1

1085 Kirkhart C, Scott K. 2015. Gustatory Learning and Processing in the Drosophila Mushroom Bod-
1086 ies. *J Neurosci* **35**:5950–5958. doi:10.1523/JNEUROSCI.3930-14.2015
1087 Kohara K, Kitamura A, Adachi N, Nishida M, Itami C, Nakamura S, Tsumoto T. 2003. Inhibitory
1088 But Not Excitatory Cortical Neurons Require Presynaptic Brain-Derived Neurotrophic
1089 Factor for Dendritic Development, as Revealed by Chimera Cell Culture. *J Neurosci*
1090 **23**:6123–6131. doi:10.1523/JNEUROSCI.23-14-06123.2003
1091 Kvon EZ, Kazmar T, Stampfel G, Yáñez-Cuna JO, Pagani M, Schernhuber K, Dickson BJ, Stark
1092 A. 2014. Genome-scale functional characterization of Drosophila developmental enhanc-
1093 ers in vivo. *Nature* **512**:91–95. doi:10.1038/nature13395
1094 Lai S-L, Awasaki T, Ito K, Lee T. 2008. Clonal analysis of Drosophila antennal lobe neurons: di-
1095 verse neuronal architectures in the lateral neuroblast lineage. *Dev Camb Engl*
1096 **135**:2883–2893. doi:10.1242/dev.024380
1097 Lai S-L, Lee T. 2006. Genetic mosaic with dual binary transcriptional systems in Drosophila. *Nat*
1098 *Neurosci* **9**:703–709. doi:10.1038/nn1681
1099 Lee T, Lee A, Luo L. 1999. Development of the Drosophila mushroom bodies: sequential gener-
1100 ation of three distinct types of neurons from a neuroblast. *Development* **126**:4065–4076.
1101 Lee T, Luo L. 1999. Mosaic analysis with a repressible cell marker for studies of gene function
1102 in neuronal morphogenesis. *Neuron* **22**:451–461.
1103 Leiss F, Groh C, Butcher NJ, Meinertzhagen IA, Tavosanis G. 2009. Synaptic organization in
1104 the adult Drosophila mushroom body calyx. *J Comp Neurol* **517**:808–824.
1105 doi:10.1002/cne.22184
1106 Lin AC, Bygrave AM, de Calignon A, Lee T, Miesenböck G. 2014. Sparse, decorrelated odor
1107 coding in the mushroom body enhances learned odor discrimination. *Nat Neurosci*
1108 **17**:559–568. doi:10.1038/nn.3660
1109 Litwin-Kumar A, Harris KD, Axel R, Sompolinsky H, Abbott LF. 2017. Optimal Degrees of Syn-
1110 aptic Connectivity. *Neuron* **93**:1153-1164.e7. doi:10.1016/j.neuron.2017.01.030
1111 Liu Z, Yang C-P, Sugino K, Fu C-C, Liu L-Y, Yao X, Lee LP, Lee T. 2015. Opposing intrinsic
1112 temporal gradients guide neural stem cell production of varied neuronal fates. *Science*
1113 **350**:317–320. doi:10.1126/science.aad1886
1114 Lovick JK, Hartenstein V. 2015. Hydroxyurea-mediated neuroblast ablation establishes birth
1115 dates of secondary lineages and addresses neuronal interactions in the developing Dro-
1116 sophila brain. *Dev Biol* **402**:32–47. doi:10.1016/j.ydbio.2015.03.005
1117 Lovick JK, Kong A, Omoto JJ, Ngo KT, Younossi-Hartenstein A, Hartenstein V. 2016. Patterns
1118 of growth and tract formation during the early development of secondary lineages in the
1119 Drosophila larval brain. *Dev Neurobiol* **76**:434–451. doi:10.1002/dneu.22325
1120 Marin EC, Watts RJ, Tanaka NK, Ito K, Luo L. 2005. Developmentally programmed remodeling
1121 of the Drosophila olfactory circuit. *Dev Camb Engl* **132**:725–737. doi:10.1242/dev.01614
1122 Marr D. 1969. A theory of cerebellar cortex. *J Physiol* **202**:437–470. doi:10.1113/jphys-
1123 iol.1969.sp008820
1124 Masuda-Nakagawa LM, Tanaka NK, O'Kane CJ. 2005. Stereotypic and random patterns of con-
1125 nectivity in the larval mushroom body calyx of Drosophila. *Proc Natl Acad Sci*
1126 **102**:19027–19032. doi:10.1073/pnas.0509643102
1127 McAllister AK, Katz LC, Lo DC. 1997. Opposing roles for endogenous BDNF and NT-3 in regu-
1128 lating cortical dendritic growth. *Neuron* **18**:767–778.
1129 McAllister AK, Lo DC, Katz LC. 1995. Neurotrophins regulate dendritic growth in developing vis-
1130 ual cortex. *Neuron* **15**:791–803. doi:10.1016/0896-6273(95)90171-X
1131 Mugnaini E, Osen KK, Dahl AL, Friedrich VL, Korte G. 1980. Fine structure of granule cells and
1132 related interneurons (termed Golgi cells) in the cochlear nuclear complex of cat, rat and
1133 mouse. *J Neurocytol* **9**:537–570.
1134 Murthy M, Fiete I, Laurent G. 2008. Testing Odor Response Stereotypy in the Drosophila Mush-
1135 room Body. *Neuron* **59**:1009–1023. doi:10.1016/j.neuron.2008.07.040

Muthukumar AK, Stork T, Freeman MR. 2014. Activity-dependent regulation of astrocyte GAT levels during synaptogenesis. *Nat Neurosci* **17**:1340–1350. doi:10.1038/nn.3791

Owald D, Waddell S. 2015. Olfactory learning skews mushroom body output pathways to steer behavioral choice in Drosophila. *Curr Opin Neurobiol* **35**:178–184. doi:10.1016/j.conb.2015.10.002

Pachitariu M, Stringer C, Dipoppa M, Schröder S, Rossi LF, Dalgleish H, Carandini M, Harris KD. 2017. Suite2p: beyond 10,000 neurons with standard two-photon microscopy. *bioRxiv* 061507. doi:10.1101/061507

Pauls D, Selcho M, Gendre N, Stocker RF, Thum AS. 2010. Drosophila larvae establish appetitive olfactory memories via mushroom body neurons of embryonic origin. *J Neurosci Off J Soc Neurosci* **30**:10655–10666. doi:10.1523/JNEUROSCI.1281-10.2010

Perkins LA, Holderbaum L, Tao R, Hu Y, Sopko R, McCall K, Yang-Zhou D, Flockhart I, Binari R, Shim H-S, Miller A, Housden A, Foos M, Randkelv S, Kelley C, Namgyal P, Villalta C, Liu L-P, Jiang X, Huan-Huan Q, Wang X, Fujiyama A, Toyoda A, Ayers K, Blum A, Czech B, Neumuller R, Yan D, Cavallaro A, Hibbard K, Hall D, Cooley L, Hannon GJ, Lehmann R, Parks A, Mohr SE, Ueda R, Kondo S, Ni J-Q, Perrimon N. 2015. The Transgenic RNAi Project at Harvard Medical School: Resources and Validation. *Genetics* **201**:843–852. doi:10.1534/genetics.115.180208

Pfeiffer BD, Truman JW, Rubin GM. 2012. Using translational enhancers to increase transgene expression in Drosophila. *Proc Natl Acad Sci U S A* **109**:6626–6631. doi:10.1073/pnas.1204520109

Pitman JL, Huetteroth W, Burke CJ, Krashes MJ, Lai S-L, Lee T, Waddell S. 2011. A Pair of Inhibitory Neurons Are Required to Sustain Labile Memory in the Drosophila Mushroom Body. *Curr Biol* **21**:855–861. doi:10.1016/j.cub.2011.03.069

Pop S, Chen C-L, Sproston CJ, Kondo S, Ramdya P, Williams DW. 2019. Patterned cell death sculpts functional and adaptive neural networks in flies. *bioRxiv* 626465. doi:10.1101/626465

Potter CJ, Tasic B, Russler EV, Liang L, Luo L. 2010. The Q System: A Repressible Binary System for Transgene Expression, Lineage Tracing and Mosaic Analysis. *Cell* **141**:536–548. doi:10.1016/j.cell.2010.02.025

Prieto-Godino LL, Silbering AF, Khallaf MA, Cruchet S, Bojkowska K, Pradervand S, Hansson BS, Knaden M, Benton R. 2019. Functional integration of “undead” neurons in the olfactory system. *bioRxiv* 623488. doi:10.1101/623488

Prokop A, Technau GM. 1994. Normal Function of the mushroom body defect Gene of Drosophila Is Required for the Regulation of the Number and Proliferation of Neuroblasts. *Dev Biol* **161**:321–337. doi:10.1006/dbio.1994.1034

Purves D. 1986. The trophic theory of neural concentrations. *Trends Neurosci* **9**:486–489. doi:10.1016/0166-2236(86)90155-4

Purves D, Hume RI. 1981. The relation of postsynaptic geometry to the number of presynaptic axons that innervate autonomic ganglion cells. *J Neurosci Off J Soc Neurosci* **1**:441–452.

Ramaekers A, Magnenat E, Marin EC, Gendre N, Jefferis GSXE, Luo L, Stocker RF. 2005. Glomerular maps without cellular redundancy at successive levels of the Drosophila larval olfactory circuit. *Curr Biol CB* **15**:982–992. doi:10.1016/j.cub.2005.04.032

Riemensperger T, Völler T, Stock P, Buchner E, Fiala A. 2005. Punishment prediction by dopaminergic neurons in Drosophila. *Curr Biol CB* **15**:1953–1960. doi:10.1016/j.cub.2005.09.042

Ruta V, Datta SR, Vasconcelos ML, Freeland J, Looger LL, Axel R. 2010. A dimorphic pheromone circuit in Drosophila from sensory input to descending output. *Nature* **468**:686–690. doi:10.1038/nature09554

1186 Shaw RE, Kottler B, Ludlow ZN, Buhl E, Kim D, Silva SM da, Miedzik A, Coum A, Hodge JJ,
1187 Hirth F, Sousa-Nunes R. 2018. In vivo expansion of functionally integrated GABAergic
1188 interneurons by targeted increase in neural progenitors. *EMBO J* e98163.
1189 doi:10.15252/embj.201798163
1190 Siller KH, Cabernard C, Doe CQ. 2006. The NuMA-related Mud protein binds Pins and regu-
1191 lates spindle orientation in Drosophila neuroblasts. *Nat Cell Biol* **8**:594–600.
1192 doi:10.1038/ncb1412
1193 Stocker RF, Heimbeck G, Gendre N, de Belle JS. 1997. Neuroblast ablation in Drosophila
1194 P[GAL4] lines reveals origins of olfactory interneurons. *J Neurobiol* **32**:443–456.
1195 Strausfeld NJ, Sinakevitch I, Brown SM, Farris SM. 2009. Ground plan of the insect mushroom
1196 body: functional and evolutionary implications. *J Comp Neurol* **513**:265–291.
1197 doi:10.1002/cne.21948
1198 Sweeney ST, Hidalgo A, Belle JS de, Keshishian H. 2012. Hydroxyurea Ablation of Mushroom
1199 Bodies in Drosophila. *Cold Spring Harb Protoc* **2012**:pdb.prot067777.
1200 doi:10.1101/pdb.prot067777
1201 Turney SG, Lichtman JW. 2012. Reversing the outcome of synapse elimination at developing
1202 neuromuscular junctions in vivo: evidence for synaptic competition and its mechanism.
1203 *PLoS Biol* **10**:e1001352. doi:10.1371/journal.pbio.1001352
1204 Vogt K, Aso Y, Hige T, Knapek S, Ichinose T, Friedrich AB, Turner GC, Rubin GM, Tanimoto H.
1205 2016. Direct neural pathways convey distinct visual information to Drosophila mushroom
1206 bodies. *eLife* **5**. doi:10.7554/eLife.14009
1207 Ward A, Hong W, Favaloro V, Luo L. 2015. Toll receptors instruct axon and dendrite targeting
1208 and participate in synaptic partner matching in a Drosophila olfactory circuit. *Neuron*
1209 **85**:1013–1028. doi:10.1016/j.neuron.2015.02.003
1210 Yagi R, Mabuchi Y, Mizunami M, Tanaka NK. 2016. Convergence of multimodal sensory path-
1211 ways to the mushroom body calyx in *Drosophila melanogaster*. *Sci Rep* **6**:29481.
1212 doi:10.1038/srep29481
1213 Yu H-H, Kao C-F, He Y, Ding P, Kao J-C, Lee T. 2010. A complete developmental sequence of
1214 a Drosophila neuronal lineage as revealed by twin-spot MARCM. *PLoS Biol* **8**.
1215 doi:10.1371/journal.pbio.1000461
1216 Zheng Z, Lauritzen JS, Perlman E, Robinson CG, Nichols M, Milkie D, Torrens O, Price J,
1217 Fisher CB, Sharifi N, Calle-Schuler SA, Kmecova L, Ali IJ, Karsh B, Trautman ET, Bo-
1218 govic JA, Hanslovsky P, Jefferis GSXE, Kazhdan M, Khairy K, Saalfeld S, Fetter RD,
1219 Bock DD. 2018. A Complete Electron Microscopy Volume of the Brain of Adult Drosoph-
1220 ila melanogaster. *Cell* **174**:730-743.e22. doi:10.1016/j.cell.2018.06.019
1221
1222